Acta Pharmaceutica Sinica B 2022;12(8):3281−3297

Chinese Pharmaceutical Association
Institute of Materia Medica, Chinese Academy of Medical Sciences

Acta Pharmaceutica Sinica B

www.elsevier.com/locate/apsb
www.sciencedirect.com

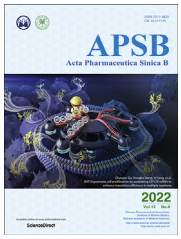

ORIGINAL ARTICLE

SYNCRIP controls miR-137 and striatal learning in animal models of methamphetamine abstinence

Baeksun Kim[a,b], Sung Hyun Tag[a,b], Eunjoo Nam[c], Suji Ham[a,b], Sujin Ahn[c], Juhwan Kim[c], Doo-Wan Cho[d], Sangjoon Lee[a,c], Young-Su Yang[d], Seung Eun Lee[e], Yong Sik Kim[f], Il-Joo Cho[b,g], Kwang Pyo Kim[h], Su-Cheol Han[d], Heh-In Im[a,b,c,*]

[a]*Convergence Research Center for Diagnosis, Treatment and Care System of Dementia (DTC), Korea Institute of Science and Technology (KIST), Seoul 02792, Republic of Korea*
[b]*Division of Bio-Medical Science & Technology, KIST School, Korea University of Science and Technology (UST), Seoul 02792, Republic of Korea*
[c]*Center for Neuroscience, KIST, Seoul 02792, Republic of Korea*
[d]*Animal Model Research Center, Jeonbuk Department of Inhalation Research, Korea Institute of Toxicology (KIT), Korea Research Institute of Chemical Technology (KRICT), Jeongeup 56212, Republic of Korea*
[e]*Research Animal Resource Center, KIST, Seoul 02792, Republic of Korea*
[f]*Department of Pharmacology, Seoul National University College of Medicine, Seoul 03080, Republic of Korea*
[g]*Center for BioMicrosystems, KIST, Seoul 02792, Republic of Korea*
[h]*Department of Applied Chemistry, Kyung Hee University, Gyeonggi-do 17104, Republic of Korea*

Received 28 September 2021; received in revised form 24 January 2022; accepted 28 January 2022

KEY WORDS

Methamphetamine;
Abstinence;
Withdrawal;
Striatum;
miR-137;
SYNCRIP;
Biomarker;
Behavior

Abstract Abstinence from prolonged psychostimulant use prompts stimulant withdrawal syndrome. Molecular adaptations within the dorsal striatum have been considered the main hallmark of stimulant abstinence. Here we explored striatal miRNA−target interaction and its impact on circulating miRNA marker as well as behavioral dysfunctions in methamphetamine (MA) abstinence. We conducted miRNA sequencing and profiling in the nonhuman primate model of MA abstinence, followed by miRNA qPCR, LC−MS/MS proteomics, immunoassays, and behavior tests in mice. In nonhuman primates, MA abstinence triggered a lasting upregulation of miR-137 in the dorsal striatum but a simultaneous downregulation of circulating miR-137. In mice, aberrant increase in striatal miR-137-dependent inhibition of SYNCRIP essentially mediated the MA abstinence-induced reduction of circulating miR-137. Pathway

*Corresponding author. Tel.: +82 2 958 6961; fax: +82 2 958 6937.
E-mail address: him@kist.re.kr (Heh-In Im).

Peer review under responsibility of Chinese Pharmaceutical Association and Institute of Materia Medica, Chinese Academy of Medical Sciences.

https://doi.org/10.1016/j.apsb.2022.02.030

modeling through experimental deduction illustrated that the MA abstinence-mediated downregulation of circulating miR-137 was caused by reduction of SYNCRIP-dependent miRNA sorting into the exosomes in the dorsal striatum. Furthermore, diminished SYNCRIP in the dorsal striatum was necessary for MA abstinence-induced behavioral bias towards egocentric spatial learning. Taken together, our data revealed circulating miR-137 as a potential blood-based marker that could reflect MA abstinence-dependent changes in striatal miR-137/SYNCRIP axis, and striatal SYNCRIP as a potential therapeutic target for striatum-associated cognitive dysfunction by MA withdrawal syndrome.

1. Introduction

Stimulant withdrawal syndrome is a type of substance-induced disorder that develops after abstinence from stimulant use/abuse[1]. Stimulant withdrawal syndrome can last from months to years after a person has quit abusing[2]. Stimulant withdrawal syndrome deserves independent clinical attention from other stimulant-induced disorders due to the severity of symptoms. However, only few studies have focused on the diagnostic and therapeutic targets selective to stimulant abstinence to date.

Stimulant abstinence causes molecular adaptations in the dorsal striatum[3,4]. Previous studies have demonstrated that striatal microRNAs (miRNAs) play a major role in the pathophysiology of stimulant abstinence[5]. miRNAs are endogenous small non-coding RNAs that inhibit the expression of target mRNA through translational repression or mRNA degradation[6]. Together, these findings suggest that the miRNA-target interaction within the dorsal striatum may be an essential component of stimulant abstinence.

Here we probed the interaction between miRNA and its target within the dorsal striatum for the theragnosis of stimulant abstinence. We aimed to identify two candidates: a stable blood-based miRNA marker that can mirror the molecular state of the dorsal striatum, and a potent therapeutic target that can reverse the behavioral symptoms induced by stimulant abstinence.

To briefly summarize, we demonstrated that abstinence from methamphetamine (MA) led to persisting inverse regulation of the brain-enriched miRNA miR-137 in the dorsal striatum and blood of nonhuman primates. The expression of blood miR-137 was directly regulated by striatal miR-137-dependent inhibition of RNA-binding protein SYNCRIP (synaptotagmin-binding cytoplasmic RNA-interacting protein; also known as HNRNP-Q or NSAP1) in mice, indicating that blood miR-137 is a mechanism-based marker of MA abstinence. In addition, rescuing SYNCRIP in the dorsal striatum normalized the MA abstinence-induced impairment in spatial navigation strategy in mice, suggesting that SYNCRIP is a novel treatment target for cognitive symptoms of MA abstinence. We propose that our study exemplifies a research pipeline for utilizing systems-level miRNA-gene interactions to identify novel theranostic targets of brain diseases.

2. Materials and methods

2.1. Study design

Sample sizes were determined on the basis of previous animal studies. Animals were randomly assigned to control and treatment groups. The investigators were blinded to allocation during experiments and outcome assessment. Biological replicates were obtained as appropriate (specific number of replicates obtained are noted in the figure legends).

2.2. Animals

2−3-year-old female cynomolgus monkeys (*Macaca fascicularis*, Korea Institute of Toxicology, Jeonbuk Branch Institute, Republic of Korea) were single-housed in stainless steel cages that permit visual, auditory, and olfactory contacts with other monkeys in a room maintained on a 12-h light/dark cycle (lights on at 8:00 AM). For each monkey, food was restricted to 120 g per 12 h while drinking water was provided *ad libitum*. Food quality and consumption amount were measured at least once per week throughout the experiment. All experimental procedures and maintenance of monkeys were conducted based on the IACUC of Korea Institute of Toxicology (KIT).

7−8-week-old male C57BL/6J mice (Daehan Bio Link, Daejeon; KIST SPF animal facility, Seoul, Republic of Korea) weighing 21−24 g were housed in groups (2−4 per cage) in clear plastic cages with wire grid lids and kept on a 12-h light/dark cycle (lights off at 7:00 AM) with *ad libitum* access to food and drinking water. All procedures regarding the use and handling of mice were conducted as approved by the Institutional Animal Care and Use Committee (IACUC) of Korea Institute of Science and Technology (KIST).

2.3. Nonhuman primate model of methamphetamine withdrawal

MA was administered in a ramp-up protocol, which mimics the gradual escalation of dose observed in human MA abusers[7,8]. The ramp-up was carried out over the course of 4 weeks as described in previous studies[9,10], with minor modifications. D-Methamphetamine hydrochloride (Ministry of Food and Drug Safety, Cheongju, Republic of Korea) was dissolved in sterile physiological saline solution (0.9%, *w*/*v*) to various concentrations (0.1−0.6 mg/mL) and stored at −80 °C until the day of experiment. Monkeys received subcutaneous (s.c.) administration of MA 1−3 times daily (s.i.d., b.i.d., or t.i.d.) for 28 days using a ramp-up protocol (0.1−0.6 mg/0.5 mL/kg).

On the 1st week, monkeys received a single injection of 0.1 mg/kg of MA on Days 1−2, 0.2 mg/kg on Days 3−4, and 0.3 mg/kg on Days 5−6. On the next week, monkeys received two injections of 0.2 mg/kg on Days 8−9, 0.3 mg/kg on Days 10−11, and 0.4 mg/kg on Days 12−13. On the 3rd week, monkeys received three injections of 0.3 mg/kg on Days 15−16, 0.4 mg/kg on Days 17−18, 0.5 mg/kg on Days 19−20. On the 4th week, monkeys received three injections of 0.6 mg/0.5 mL/kg daily. MA

was administered at 10:00, 13:00, and 16:00 each. Injections were given at four different subscapular areas in serial order to avoid potential irritation from multiple needle penetrations into the same injection site.

Clinical parameters were examined throughout the study. Clinical signs were observed at least once daily for potential complications. A hematological test was conducted on Day 26 (during MA exposure) and Day 82 (during MA withdrawal) of the protocol, and the examined parameters were within normal range. At the day of necropsy, monkeys were euthanized with a lethal dose of thiopental sodium (250 mg/5 mL/monkey).

2.4. Mouse model of methamphetamine withdrawal

MA was administered according to the ramp-up protocol over the course of 4 weeks as described in previous studies[11], with minor modifications. D-Methamphetamine hydrochloride was dissolved in sterile physiological saline solution to various concentrations (0.1−0.8 mg/mL) and stored at −80 °C until the day of the experiment. Mice received intraperitoneal (i.p.) administration of MA 1−3 times daily (s.i.d., b.i.d., or t.i.d.) for a total of 14 days by the previously described ramp-up protocol (0.5−4.0 mg/5.0 mL/kg). MA was administered at 13:00, 15:00, and 17:00 each.

On Days 1−3, mice received a single injection of 0.5, 1.0, and 1.5 mg/kg of MA, respectively. On Days 4−6, mice received two injections of 1.5, 2.0, and 2.5 mg/kg of MA. On Days 8−10, mice received three injections of 2.5, 3.0, and 3.5 mg/kg of MA. On Days 11−13, mice received three injections of 4.0 mg/kg of MA daily. Injections were given at two different areas in serial order to avoid potential irritation from multiple needle penetrations onto the same injection site. Mice were sacrificed at 1, 3, and 6 weeks after the last day of MA exposure protocol.

2.5. Blood and brain sample preparation

Mice were deeply anesthetized by i.p. administration of Avertin (2,2,2-tribromoethanol, 250 mg/20 mL/kg; Sigma−Aldrich). Whole blood was collected by venipuncture, and left at room temperature (RT) for 20 min for coagulation before centrifugation at 2000 × *g* for 15 min at 4 °C. The supernatant (serum) was collected and immediately subjected to extracellular vesicle (EV) isolation (described in the next section). Then, the whole brain was quickly isolated, frozen in dry ice and stored at −80 °C. Later, frozen brains were coronally sectioned on a cryostat (CM3050S, Leica Microsystems, Wetzlar, Germany) to a thickness of 150 μm at −20 °C and then further dissected with cold surgical micro-knife to isolate the regions of interest.

In monkeys, blood was drawn at 20 min after the last administration of MA during the MA exposure period to examine the acute effect of MA exposure (while MA remains in the physiological system), and at the beginning of the light cycle (between 9:00−10:00 AM) during the withdrawal period to examine the long-lasting effect of MA exposure (while MA has been washed out from the system). Blood samples were immediately subjected to serum isolation followed by EV isolation as described previously.

Fresh brains were quickly isolated, weighed, and then immediately frozen in dry ice and stored at −80 °C. Frozen brains were coronally sectioned on a cryostat to a thickness of 150 μm at −20 °C and then further dissected with cold surgical micro-knife to isolate the regions of interest.

2.6. Circulating extracellular vesicles

ExoQuick (System Biosciences, Mountain View, CA, USA) was used for isolation of circulating EVs (cEVs). An appropriate amount of ExoQuick was mixed with the serum samples following the manufacturer's protocol. Then the mixture was refrigerated at 4 °C for 1 h and centrifuged at 2000 × *g* for 15 min. The supernatant was removed by aspiration, and pelleted fraction (cEV) was resuspended in either DEPC-DW or cold 1 × PBS for RNA isolation or transmission electron microscopy, respectively.

To study the stability of miRNA in the circulating extracellular vesicles, the temperature-dependent degradation of cEV miRNA was analyzed, where EVs were kept at 25 or 37 °C for 24 h. For analyzing RNase-dependent degradation of cEV miRNA, EV samples were incubated with RNase A (10 μg/mL, Sigma−Aldrich) or RNase with Triton X-100 (1%, Sigma−Aldrich). The stability of EV cargo was analyzed by measuring cycle threshold (Ct) value of miR-16 through quantitative real-time PCR (qPCR).

2.7. Brain extracellular vesicle isolation by PROSPR

EVs from brain tissue was isolated *via* Protein Organic Solvent Precipitation (PROSPR) method as described previously[12], with minor modification. Briefly, whole dorsal striatum was isolated from mice and collected in a 1.5 mL microcentrifuge tube. Then the dorsal striatum was homogenized in 200 μL of 100 mmol/L ammonium acetate buffer (pH 6.5) supplemented with RNase inhibitor (Thermo Fisher Scientific, Waltham, MA, USA) and protease inhibitor cocktail (Thermo Fisher Scientific), centrifuged at 16,000 × *g* for 10 min and the supernatant was collected in 15 mL conical tube. The homogenization to collection step was repeated four times with increasing power of homogenization.

Then, all supernatant samples were combined and four volumes of −20 °C acetone was added, immediately vortexed for 5 s, and then centrifuged at 6000 × *g* for 45 s. The supernatant was immediately collected and dehydrated in a vacuum concentrator for 2 h (CC-105, Tomy Seiko, Tokyo, Japan). The dehydrated pellets were used for RNA isolation followed by miRNA qPCR.

2.8. Transmission electron microscopy

cEVs from naïve mice were fixed with 1% (*v*/*v*) glutaraldehyde for 1 h at room temperature, layered onto formvar-coated 200 mesh copper grids (ProSciTech, Queensland, Australia), and left to dry at room temperature. Grids were then washed twice with water for 5 min and stained with 1% (*w*/*v*) uranyl acetate in water for 10 min. Imaging was performed at an acceleration voltage of 200 kV using Gatan Ultra Scan 1000 (2 × 2k) CCD (charge-coupled device) camera coupled to Tecnai F30 (Philips-FEI, Eindhoven, Netherlands) electron microscope. Images of 10 different areas of grids were captured, followed by computer image analysis using ImageJ (National Institute of Health, Bethesda, MD, USA). After setting the scale of the images, the amount and individual size of vesicles in the images were measured in each sample. Incomplete vesicles located at the edge of the images were excluded.

2.9. Raman spectroscopy

For Raman spectroscopy, EV and EV-depleted serum (EDS) fractions were separated from whole sera of naïve mice and the

EV fraction was diluted in 20 μL of 1 × PBS. Raman spectroscopy data were obtained using inVia system (Renishaw, Gloucestershire, UK) at room temperature using a Nd:YAG laser with an excitation wavelength of 532 nm. Raman spectra were obtained at 1 s exposure and 200 accumulations to reduce the signal-to-noise ratio. All measurements were performed with 50 × objective lens, slit opening 65 μm and centre 1880 μm, grating 2400 L/mm. For analyses of spectral bands pertaining to nucleic acids (750−850 cm^{-1}), Amide I protein (1600−1690 cm^{-1}), and lipids (2750−3040 cm^{-1}), measurements were taken at spectral ranges 700−1850 cm^{-1} and 2300−3200 cm^{-1} centered at 1300 and 2800 cm^{-1}, respectively.

2.10. miRNA sequencing

Total RNA from carefully microdissected caudate/putamen of nonhuman primates were isolated after MA withdrawal for next-generation sequencing of miRNAs. RNA quality was assessed by $OD_{260/280}$ and $OD_{260/230}$ values measured from NanoDrop 2000 UV−Vis Spectrophotometer (Thermo Fisher Scientific), migration patterns visualized by electrophoresis, peak patterns from electropherogram, and RNA Integrity Number (RIN) measured by 2100 Bioanalyzer Instrument (Agilent Technologies, CA, USA). Library construction was carried out using NEBNext Small RNA Library Prep Set for Illumina (New England Biolabs, MA, USA), and miRNA expression was profiled using NextSeq500 (Illumina, CA, USA). Raw data were normalized by global normalization between samples.

2.11. Lentiviral expression

Human pre-microRNA Expression Construct Lenti-miR-137 (PMIRH137PA-1, System Biosciences), miArrest miRNA inhibitor against hsa-miR-137 (HmiR-AN0175-AM04p, GeneCopoeia, MD, USA), and Syncrip (NM_019,666) mouse tagged ORF clone (MR217725L4, OriGene Technologies, MD, USA) were used for lentiviral expression of miR-137, antagomir of miR-137, and SYNCRIP, respectively. For each lentivector, an appropriate control lentivector was used according to the manufacturer's recommendation.

Each vector was packaged into lentivirus using Lenti-Pac HIV Expression Packaging Kit (System Biosciences) according to the manufacturer's protocol. Viral suspension concentrations ranged from 1.0×10^9−3.0×10^9 infectious units per ml (IFU/mL).

2.12. Intrastriatal microinfusion

For the intrastriatal infusion of lentivirus, mice were anesthetized by i.p. administration of ketamine−xylazine mixture (120 and 8 mg/kg, respectively) and appropriately positioned in a stereotaxic frame (Kopf Instruments, CA, USA). Microinfusions were delivered into both hemispheres of the dorsal striatum at the following stereotaxic coordinates: anteroposterior (AP) +1.2 mm; mediolateral (ML) ±1.65 mm from midline; dorsoventral (DV) −3.1, −2.7 and −2.3 mm below dura. Microinfusion was carried out by NE-4000 Programmable 2 Channel Syringe Pump (New Era Pump Systems, NY, USA). Three microinfusions were delivered into each hemisphere of the dorsal striatum, with the infusion volume of 0.2, 0.7, and 0.7 μL per each coordinate. The infusion rate was 0.1 μL/min. After each infusion, the microneedle was held in position for 2 min.

2.13. Immunohistochemistry

Mice were deeply anesthetized with Avertin as described previously. Then, transcardial perfusion was performed with 1 × PBS followed by 4% paraformaldehyde (PFA) in 1 × PBS. The whole brain was isolated, post-fixed in 4% PFA for overnight at 4 °C, dehydrated with 30% sucrose until submersion, embedded in OCT compound and stored at −80 °C until cryosectioning.

For immunohistochemistry, OCT-embedded brains were coronally sectioned on a cryostat to a thickness of 40 μm at −20 °C. Free-floating sections were rinsed in 1 × PBS followed by 0.3% Triton X-100 in 1 × PBS (PBST). Washed sections were blocked with 5% normal donkey serum (NDS) in PBST for 1 h, then the sections were incubated with rabbit anti-GFP (1:500, sc-8334, Santa Cruz Biotechnology) or rabbit anti-DsRed (1:500, #632496, Takara Bio, Shiga, Japan) in 1% NDS for overnight at 4 °C. Subsequently, the sections were washed and incubated with donkey anti-rabbit IgG Alexa Fluor 488 (1:400) or donkey anti-rabbit IgG Alexa Fluor 594 (1:400, Thermo Fisher Scientific) for 2 h at RT. Finally, the sections were washed and mounted with VECTASHIELD HardSet Antifade Mounting Medium with DAPI (Vector Laboratories, CA, USA) according to the manufacturer's protocol. Images were taken with FluoView FV1000 (Olympus, Tokyo, Japan) and processed using FluoView software (Olympus), then the images were visualized using Zen software (Carl Zeiss, Oberkochen, Germany).

2.14. RNA immunoprecipitation

RNA immunoprecipitation was performed with Magna RIP™ RNA-Binding Protein Immunoprecipitation Kit (Merck Millipore, Darmstadt, Germany) according to the manufacturer's protocol. 5 μL of rabbit anti-SYNCRIP (ab184946, Abcam, Cambridge, UK) was used per reaction. miRNA fold change in the RNA immunoprecipitation samples was expressed as the percentage of the input and compared to IgG isotypic control.

2.15. RNA extraction

Total RNA from brain or EV samples was isolated using RNA STAT-60 (AMS Biotechnology, Abingdon, UK) or TRIzol reagent (Thermo Fisher Scientific, MA, USA) according to the manufacturer's protocol. RNA yield and quality were determined using NanoDrop 2000 UV−Vis Spectrophotometer (Thermo Fisher Scientific).

2.16. Quantification of mature RNAs

50 ng of total RNA from each sample (20 ng of total RNA for brain EV samples and RNA immunoprecipitation samples) was used for cDNA preparation through reverse transcription. For miRNAs, cDNA was amplified using TaqMan Universal Master Mix II, no UNG (Thermo Fisher Scientific) according to the manufacturer's protocol. Thereafter, the expression of mature miRNAs was quantified using qPCR with TaqMan MicroRNA Assays (Thermo Fisher Scientific). qPCR reactions were run on CFX connect (Bio-Rad). All reactions were performed in triplicates.

The relative abundance of miRNAs was calculated by $2^{-\Delta\Delta Ct}$ method[13]. snoRNA202 and RNU66 were used as normalization controls for brain miRNA quantification in mice and nonhuman primates, respectively. The reference miRNA miR-16 was used as a normalization control for cEV and brain EV miRNA quantification.

2.17. Luciferase assay

miRNA 3′UTR target expression clone for Mouse Syncrip NM_019666.2 (SYNCRIP-3′UTR) (MmiT031985-MT05, GeneCopoeia), human pre-microRNA expression construct Lenti-miR-137 (PMIRH137PA-1, System Biosciences), and appropriate control vectors were used for luciferase assay. Briefly, SYNCRIP-3′UTR or SYNCRIP-3′UTR mutant vector was transfected together with miR-137 overexpression vector or a scrambled control vector to HEK293TN cells in 12-well cell culture plate using EndoFectin Lenti transfection reagent (GeneCopoeia) according to the manufacturer's protocol. Media was changed 16 h after transfection and collected 48 h after transfection.

For each well, the activity of *Gaussia luciferase* was normalized to the activity of secreted alkaline phosphatase using Secrete-Pair Dual Luminescence Assay Kit (GeneCopoeia) according to the manufacturer's protocol. Each enzyme's activity was quantified by obtaining absorbance readings with the Synergy HTX Multi-Mode Microplate Reader (BioTek, VT, USA).

2.18. Proteomic identification and analysis of miR-137-bound proteins

2.18.1. miRNA-protein pull-down assay

miR-137-bound proteins were isolated using Pierce Magnetic RNA−Protein Pull-Down Kit (Thermo Fisher Scientific) according to the manufacturer's protocol. 3′-End desthiobiotinylated miR-137 was synthesized (Bioneer, Daejeon, Republic of Korea) and used as the target RNA. Protein was sampled from the whole brain of a wild-type C57BL/6J mouse to achieve the protein concentration necessary for RNA−protein pull-down assay. The isolated miR-137-bound proteins were electrophoresed in a running gel and then visualized by staining with Coomassie Brilliant Blue R-250 (Thermo Fisher Scientific). The whole gel was subsequently destained and immediately subjected to in-solution digestion with trypsin and LC−MS/MS analysis (ProteomeTech Inc., Seoul, Republic of Korea) as described below.

2.18.2. In-solution digestion with trypsin and extraction of peptides

Sample gel was reduced and alkylated. In-solution digestion was done using sequencing grade trypsin enzyme:substrate ratio (E/S) of 1:20 at 37 °C overnight. The tryptic peptides were subjected to a desalting process using a reversed-phase column[14]. Briefly, after an equilibration step with 0.1% formic acid, the peptides solution was loaded on the column and washed with 0.1% formic acid. The bound peptides were eluted with 70% acetonitrile with 0.1% formic acid.

2.18.3. Identification of proteins by LC−MS/MS

LC−MS/MS analysis was performed through nanoACQUITY UPLC and LTQ-orbitrap-mass spectrometer (Thermo Electron, CA, USA). The column used BEH C18 column (1.7 μm, 100 μm × 100 mm, Waters corp., MA, USA). The mobile phase A for the LC separation was 0.1% formic acid in deionized water and the mobile phase B was 0.1% formic acid in acetonitrile. The chromatography gradient was set up to give a linear increase from 5% B to 40% B for 60 min, from 40% B to 95% B for 5 min, 95% B for 9 min, and subsequent decline from 95% B to 5% B for 1 min and 5% B for 15 min. The flow rate was 0.3 μL/min. For tandem mass spectrometry, mass spectra were acquired using data-dependent acquisition with full mass scan (*m/z* 300−2000) followed by MS/MS scans. Each MS/MS scan acquired was an average of one microscans on the LTQ. The temperature of the ion transfer tube was controlled at 275 °C and the spray was 2.0 kV. The normalized collision energy was set at 35% for MS/MS. The individual spectra from MS/MS were processed using the SEQUEST software (Thermo Quest, CA, USA) and the generated peak lists were used to query in house database using the MASCOT program[15] (Matrix Science Ltd., London, UK). We set the modifications of carbamidomethyl (C), deamidated (NQ), oxidation (M) for MS analysis and the tolerance of peptide mass was 10 ppm. MS/MS ion mass tolerance was 0.8 Da, allowance of missed cleavage was 2, and charge states (+2, +3) were taken into account for data analysis. We took only significant hits as defined by MASCOT probability analysis.

2.18.4. Analysis of miR-137-bound proteins

From a total of 273 putative miR-137-bound peptides, we isolated a total of 242 peptides with MASCOT ions score above 40 (Matrix Science; www.matrixscience.com). Subsequently, a total of seven proteins were identified to be RNA-binding proteins according to exhaustive literature search. Lastly, only one protein was predicted to be targeted by miR-137 in both TargetScan v7.2[16] and DIANA microT-CDS v5.0[17].

2.19. Immunoblot

Protein from brain or cell samples was extracted using RIPA buffer (Thermo Fisher Scientific) according to the manufacturer's protocol. Protein samples were quantified by Bradford assay using Protein Assay Dye Reagent Concentrate (Bio-Rad) and spectrophotometer.

Protein (50 μg/lane in general; 5 μg/lane for albumin immunoblot) was separated by mass using SDS-PAGE and transferred onto PVDF membranes. Membranes were blocked with 5% skim milk for 1 h, washed, and was then incubated with primary antibodies: rabbit anti-CD63 (1:500, ab216130, Abcam), mouse anti-GAPDH (1:1000, sc-47724, Santa Cruz Biotechnology, CA, USA), rabbit anti-ApoA1 (1:500, ab227455, Abcam), rabbit anti-albumin (1:1000, ab222923, Abcam), rabbit anti-SYNCRIP (1:10,000, ab184946, Abcam) and mouse anti-β-actin (1:500, sc-47778, Santa Cruz Biotechnology) for overnight at 4 °C followed by 2 h at RT. Subsequently, membranes with bound primary antibodies were washed and incubated with donkey anti-rabbit IgG-HRP (1:2000, sc-2317, Santa Cruz Biotechnology) or donkey anti-mouse IgG-HRP (1:2000, sc-2318, Santa Cruz Biotechnology) for 2 h at RT. HRP signal was visualized using SuperSignal West Pico Chemiluminescent Substrate (Thermo Fisher Scientific) and Image Quant LAS4000 (GE Healthcare Bio-Sciences, Uppsala, Sweden).

Quantitative densitometric comparisons between samples were carried out using ImageJ. Samples from same blots in an experiment were processed in parallel and loading control (β-actin) was run on the same blot as the target (SYNCRIP). Within an experiment, all experimental and control samples were analyzed.

2.20. Behavior

Mice were habituated in the behavior room for 30 min before the behavior assay. Behavioral sessions were video-recorded for analysis.

2.20.1. Open field

A white open field arena (40 cm × 40 cm × 40 cm inner dimension) with ~5 lux luminosity on the floor was used. After placing mice facing one side of the wall in the open field, the mice were allowed to freely explore the arena for 20 min. The distance moved (cm) and the time spent in the center zone (s) were analyzed using EthoVision XT 11.5 (Noldus, Wageningen, Netherlands).

Rearing and circling were counted manually. Circling was defined as the mouse traveling through the walls of the open field in full circle for more than 10 s without stopping for >2 s, making a change of direction (*e.g.*, clockwise to counterclockwise or *vice versa*, or entering the center zone), or rearing. 10 s of continuous circling was counted as one episode of circling.

2.20.2. Rotarod

Before beginning of the first session of the rotarod test, mice were acclimated on the rotarod with a fixed rate of 4 rpm for 5 min. The rotarod test was conducted two times per day for a total of two days, with a 1-h inter-session interval. Within a session, mice were subjected to two consecutive trials of the rotarod test (total of four trials/day). In a trial, mice were subjected to 4 rpm fixed-speed training for 30 s on the rotarod and then were immediately subjected to acceleration (from 4 to 30 rpm, accelerating over 5 min). Latency to fall (s) was measured for each trial, and normalized to the first session of the Control-Veh group (mice that received intrastriatal control lentivirus infusion and intraperitoneal vehicle injection).

The within-group, learning-mediated enhancement in motor skill (motor learning index) was calculated according to the previous study[18]. The motor learning index was defined as the average of latency to fall within a session normalized to the average of the latency to fall in the first session, expressed in percentage.

2.20.3. Water cross maze (WCM)

A cross-shaped maze with 40 cm-long, 10 cm-wide arms and 30 cm depth was used as the testing apparatus. Clear, invisible Plexiglass platform was placed on one arm of the maze. Opposite of the start arm was blocked by clear, invisible acrylic Plexiglass guillotine door (schematic illustration shown in Fig. 5A). Mice passed through a total of 48 trials during acquisition/reversal. Acquisition and reversal phases were separated by 3 days. Acquisition/reversal consisted of two sessions per day with an inter-session interval of 3 h, and three trials/session with inter-trial interval of 5 min (total six trials per day). Probe trial was conducted on the 4th day of acquisition/reversal, on the 3rd trial of the six trials conducted on the probe test day.

During the learning trials, mice were placed facing the end of the start arm, and were allowed to use both intramaze visual cues and body turns to solve a trial for 60 s. A trial was scored accurate when the mouse (1) climbed onto the hidden platform within 10 s, and (2) did not select the arm opposite to the hidden platform. Arm selection was counted when the whole body of the mouse crossed the midpoint of an arm.

Mice were considered having learned when the accuracy reached ≥80% on the 4th day of acquisition/reversal, and mice that failed to learn the location of the hidden platform in either acquisition/reversal phase were excluded from analysis. Two out of 62 mice were dropped from the study based on the exclusion criterion (one from $DST^{SYNCRIP\text{-}OE}$ group and one from MA abstinence group).

During the probe trials, mice were placed facing the end of the arm opposite to the start arm, and were allowed to freely explore the maze for 60 s. The navigation strategy of a mouse was considered allocentric if the mouse selected the arm that had hidden platform, and egocentric if the mouse selected the arm opposite to the hidden platform. In addition, the decision latency (latency to select an arm) and change-of-mind decisions (trials in which mice entered an arm but turned around before the midpoint and selected the opposite arm) were recorded.

2.21. Statistics

For striatal miRNA sequencing data of nonhuman primates, random sampling with replacements (bootstrapping) was conducted[19]. Bootstrap *P*-value was calculated by analyzing 100,000 repetitions of bootstrap dataset. Linear regression was used to question whether the slope is significantly non-zero in the relationship between two variables in XY scatter plots. Fisher's exact test was used to compare the proportion of navigation strategy selected during "Change-of-mind" decisions *versus* "Stay" decisions. Student's *t*-test, one-way analysis of variance (ANOVA) followed by Holm-Sidak's *post-hoc* test, and two-way ANOVA followed by either Fisher LSD *post-hoc* test or Holm-Sidak's *post-hoc* test were conducted when appropriate. For all empirical tests, $P < 0.05$ was considered statistically significant. Significance was denoted as $^{*}P < 0.05$, $^{**}P < 0.01$, $^{***}P < 0.001$, and $^{****}P < 0.0001$ unless noted otherwise. Data were displayed as mean ± standard error of the mean (SEM) unless noted otherwise. All statistical analyses were conducted with Prism v6.0 (GraphPad, CA, USA) and Microsoft Excel.

3. Results

3.1. MA abstinence oppositely regulates striatal and circulating miR-137

Previous studies demonstrated that substance-induced disorder can perturb microRNA (miRNA) dynamics within the brain. Here, we sought to identify a stable miRNA signature of methamphetamine (MA) abstinence in a nonhuman primate model (Fig. 1A; Supporting Information Table S1). Through quantitative expression profiling of evolutionarily conserved and brain-enriched miRNAs[20], we found that three miRNA candidates were upregulated in the caudate/putamen even after eight weeks of MA abstinence (Fig. 1B). Follow-up qPCR validation revealed that the expression of miR-137 was significantly enhanced in the caudate/putamen after MA abstinence, while other miRNAs were unchanged (Fig. 1C).

Extracellular vesicles (EVs) are cell-derived, lipid-bound structures secreted into the extracellular space[21]. EVs readily cross the blood−brain barrier and stably carry miRNAs throughout circulation[22,23]. Therefore, the MA abstinence-induced increase in striatal miR-137 may be mirrored in the circulating extracellular vesicles (cEVs), yielding a stable blood-based marker of MA abstinence.

First, we determined whether the cEVs can stably transport miRNAs throughout circulation (Supporting Information Fig. S1). Following previously established guidelines[24,25], the size distribution of isolated cEV fractions was characterized through transmission electron microscopy (Fig. S1A and S1B). Nearly 70% of all EVs were <100 nm in diameter as in a previous

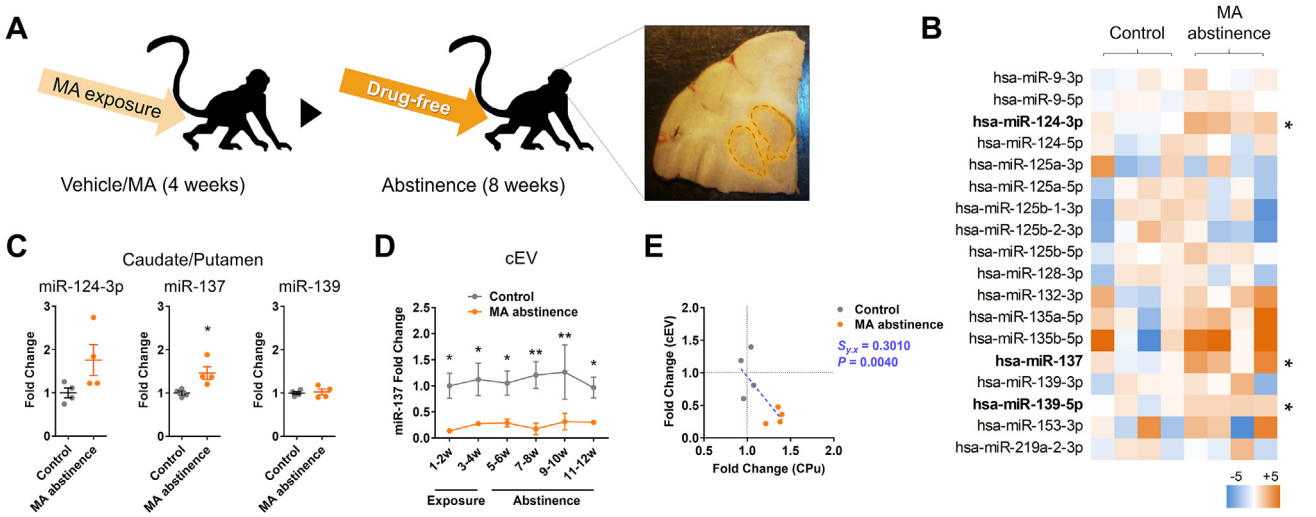

Figure 1 MA abstinence triggers opposite regulation of striatal and circulating miR-137. (A) Simplified schedule for modeling of methamphetamine (MA) abstinence in nonhuman primates (n = 4/group). Image on the right shows the coronal brain section containing the whole striatum, with orange-colored boundary indicating the caudate/putamen (CPu). (B) Heatmap of brain-enriched miRNA expression levels in the caudate/putamen of MA-withdrawn nonhuman primates. Bold marks indicate significantly altered miRNAs (Bootstrap t-test). Gene expression was saturated at −5 and +5 levels of fold change for visualization. (C) qPCR validation revealed that miR-137 was significantly upregulated in the caudate/putamen in response to MA abstinence, while miR-124-3p and miR-139 were not (Student's t-test). (D) miR-137 was persistently diminished in the circulating extracellular vesicles (cEVs) throughout MA abstinence (Fisher LSD *post-hoc* comparison). (E) XY scatter plot with linear regression showed that MA abstinence causes an inverse regulation of miR-137 in the CPu and cEVs in nonhuman primates (linear regression). All error bars represent standard error of the mean. All qPCR experiments were repeated at least once.

study[26], which indicates that the majority of the cEVs were of the size generally described for exosomes. Next, the contents of cEVs were defined through Raman spectroscopy (Fig. S1C). The nucleic acid-to-lipid ratio as well as protein-to-lipid ratio were substantially higher for the cEVs than the EV-depleted serum (EDS) fraction, suggesting that the cEV fraction is enriched with genetic materials. Lastly, the purity of cEVs was assessed through immunoblotting of EV-positive and EV-negative markers (Fig. S1D). The EV-positive markers GAPDH and CD63 were isolated within the cEVs but not EDS, suggesting that the cEVs were isolated with high sensitivity. On the other hand, the EV-negative markers ApoA1 and albumin were co-isolated with cEVs, suggesting that the cEV fraction contained impurity. However, the amount of EV-negative markers was substantially smaller in the cEVs compared to the EDS.

Subsequently, we checked whether the cEVs can protect the enveloped miRNA from temperature- and RNase-dependent degradation. Here we measured the expression level of miR-16, a reference EV miRNA with notable stability across different storage conditions[27]. cEV miR-16 was rapidly degraded at body temperature (37 °C) than at standard ambient temperature (25 °C) (Fig. S1E, above), but the degradation rate was significantly lower in the cEVs than in the EDS (Fig. S1E, below). Next, after incubation with RNase, we found that the cEVs were able to protect miR-16 from RNase-dependent degradation (Fig. S1F), as detergent-mediated lysis of EVs led to significant degradation of miR-16 by RNase. These data demonstrate that cEVs are a stable carrier of miRNAs in circulation.

We anticipated cEV miR-137 to mirror the expression pattern of striatal miR-137. Unexpectedly, cEV miR-137 expression was persistently diminished throughout MA abstinence in the nonhuman primate model (Fig. 1D), and linear regression analysis indicated that striatal miR-137 was negatively correlated with circulating miR-137 (Fig. 1E). These results suggest that miR-137 is oppositely altered in the dorsal striatum and cEVs during MA abstinence.

3.2. *Increase in striatal miR-137 is sufficient and necessary for the reduction of circulating miR-137*

The results from the nonhuman primate model of MA abstinence led us to speculate that causality could exist between the elevation of striatal miR-137 and the reduction of cEV miR-137 during the protracted abstinence from MA. To explore this possibility, experimental manipulation of striatal miR-137 during MA abstinence was essential.

We therefore generated a mouse model of MA abstinence (Fig. 2A; Supporting Information Table S2). In the mouse model, striatal miR-137 was upregulated while cEV miR-137 was decreased through 1−6 weeks of MA abstinence (Fig. 2B and C), which recapitulated the findings from the nonhuman primate model of MA abstinence. Also, striatal miR-137 was negatively correlated with cEV miR-137 in the mouse model (Fig. 2D).

Next, we investigated whether the increase in striatal miR-137 was necessary for the MA abstinence-induced reduction of cEV miR-137. Through lentivirus microinjection, miR-137 was knocked down in the whole striatal cell population of the mouse model of MA abstinence ($DST^{miR137\text{-}KD}$; Fig. 2E), while other groups of mice received control lentivirus infusion. Quantitative expression analysis demonstrated that $DST^{miR137\text{-}KD}$ was effective at reversing the MA abstinence-dependent increase in striatal miR-137 (Fig. 2F), and also at rescuing the MA abstinence-induced deficit in cEV miR-137 (Fig. 2G). Additionally, cEV miR-137 was still inversely correlated with striatal miR-137 (Fig. 2H). Moreover, $DST^{miR137\text{-}KD}$ in naïve mice was sufficient to reduce cEV miR-137 (Supporting Information Fig. S2).

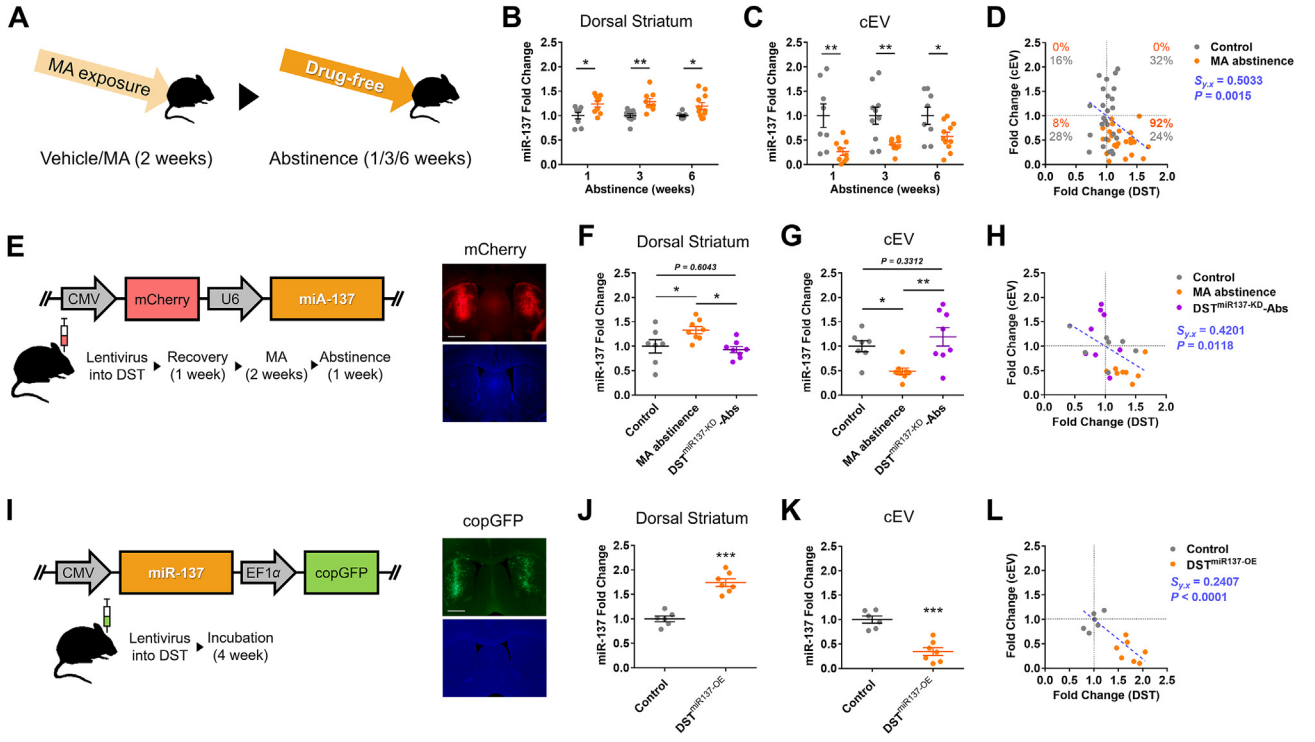

Figure 2 Increase in striatal miR-137 is causally linked to decrease in circulating miR-137. (A) Simplified schedule for modeling MA abstinence in mice (n = 8−11/group). (B) miR-137 in the dorsal striatum was significantly and persistently enhanced throughout the duration of six weeks of abstinence from methamphetamine (MA) (orange dots) compared to the control (grey dots) (Fisher LSD *post-hoc* test). (C) Circulating extracellular vesicle (cEV) miR-137 was significantly and persistently reduced through 1−6 weeks of abstinence (orange dots) compared to the control (grey dots) (Fisher LSD *post-hoc* test). (D) MA abstinence led to opposing expression patterns of miR-137 between the dorsal striatum (DST) and cEVs in mice (linear regression). Majority of the values in MA group (92%) were concentrated in the IV quadrant. All data points from one to six weeks of MA abstinence were pooled. (E) Schedule for lentivirus-mediated knock-down of miR-137 in the dorsal striatum ($DST^{miR137\text{-}KD}$) of MA-abstinent mice (n = 7−8/group). Images show immunohistochemical confirmation of lentiviral expression in the mouse DST. Scale bar in the image indicates 1 mm. (F) Increase in DST miR-137 was rescued by $DST^{miR137\text{-}KD}$ in the MA-abstinent mice (Holm-Sidak's *post-hoc* test). (G) Decrease in cEV miR-137 was rescued by $DST^{miR137\text{-}KD}$ in the MA-abstinent mice (Holm-Sidak's *post-hoc* test). (H) miR-137 was oppositely regulated in the brain and blood by $DST^{miR137\text{-}KD}$ (linear regression). (I) Schedule for lentivirus-mediated overexpression of miR-137 in the dorsal striatum ($DST^{miR137\text{-}OE}$) of naïve mice (n = 6−7/group). Images show immunohistochemical confirmation of $DST^{miR137\text{-}OE}$ in the mouse DST. White bar in the image indicates 1 mm. (J) qPCR confirmation of $DST^{miR137\text{-}OE}$ (Student's t-test). (K) $DST^{miR137\text{-}OE}$ led to significant reduction of cEV miR-137 (Student's t-test). (L) $DST^{miR137\text{-}OE}$ led to opposing expression patterns of miR-137 in DST and cEVs (linear regression). All values in MA abstinence group were concentrated in the IV quadrant. All error bars represent standard error of the mean. All qPCR experiments were repeated at least once.

Then, we investigated whether the increase in striatal miR-137 was sufficient for the reduction of cEV miR-137. As expected, lentiviral overexpression of striatal miR-137 in naïve mice ($DST^{miR137\text{-}OE}$; Fig. 2I and J) caused the reduction of cEV miR-137 (Fig. 2K), and the expression patterns of miR-137 exhibited strong inverse correlation in the brain and blood (Fig. 2L).

Together, these data demonstrate that the expression pattern of cEV miR-137 is causally associated with the expression pattern of striatal miR-137 in MA-abstinent animals, and that there exists a biological mechanism for brain-dependent regulation of circulating miRNAs.

Additionally, we also examined whether the abstinence from single MA exposure perturbs miR-137 in the dorsal striatum and cEVs (Supporting Information Fig. S3A). We found that both striatal and cEV miR-137 were unaffected by abstinence from single MA treatment (Fig. S3B−S3D), suggesting that abstinence from chronic, but not acute, exposure to MA leads to aberrant regulation of miR-137 in the brain and blood.

Furthermore, we checked whether MA abstinence altered miR-137 in brains regions other than the dorsal striatum. In nonhuman primates and mice, miR-137 was quantified in the nucleus accumbens, the essential brain region for reward processing and drug addiction[28]. Additionally, miR-137 was assessed in other four large brain structures of mice (neocortex, hippocampus, thalamus, cerebellum), in which bulk release of EVs could heavily influence the contents of circulating RNAs. We found that miR-137 was not altered by MA abstinence in the nucleus accumbens, cortex, hippocampus, thalamus, and cerebellum of animal models (Supporting Information Fig. S4A and S4B), suggesting that miR-137 may be specifically dysregulated in the dorsal striatum during MA abstinence.

Lastly, we assessed striatal miR-124-3p and miR-139, the miRNAs that were putatively altered in non-human primate striatal miRNA-seq (Fig. 1B), in the mouse model of MA abstinence. We found that miR-124-3p and miR-139 were not significantly altered in the dorsal striatum of mice after MA abstinence (Fig. S4C and S4D).

3.3. *The RNA-binding protein SYNCRIP bidirectionally interacts with miR-137*

miRNAs play an important role in regulating mRNA expression by post-translational repression[6]. Therefore, we speculated that one of the target genes of striatal miR-137 may be responsible for the MA abstinence-induced reduction of cEV miR-137. Here, we conjectured that the target gene of miR-137 could be an RNA-binding protein that controls miRNA sorting into the EVs[29,30]. In this model, (1) striatal miR-137 would repress the expression of the miRNA-sorting protein, (2) inhibit the transport of miR-137 into the EVs, and (3) reduce the amount of EV miR-137 released into the circulation.

To test this model, we first analyzed striatal miR-137-bound proteins by RNA−protein pulldown and LC−MS/MS proteomics. A total of 242 proteins were identified as interaction modules of miR-137 (Fig. 3A; Supporting Information Table S3), among which fragments of seven proteins were classified as RNA-binding

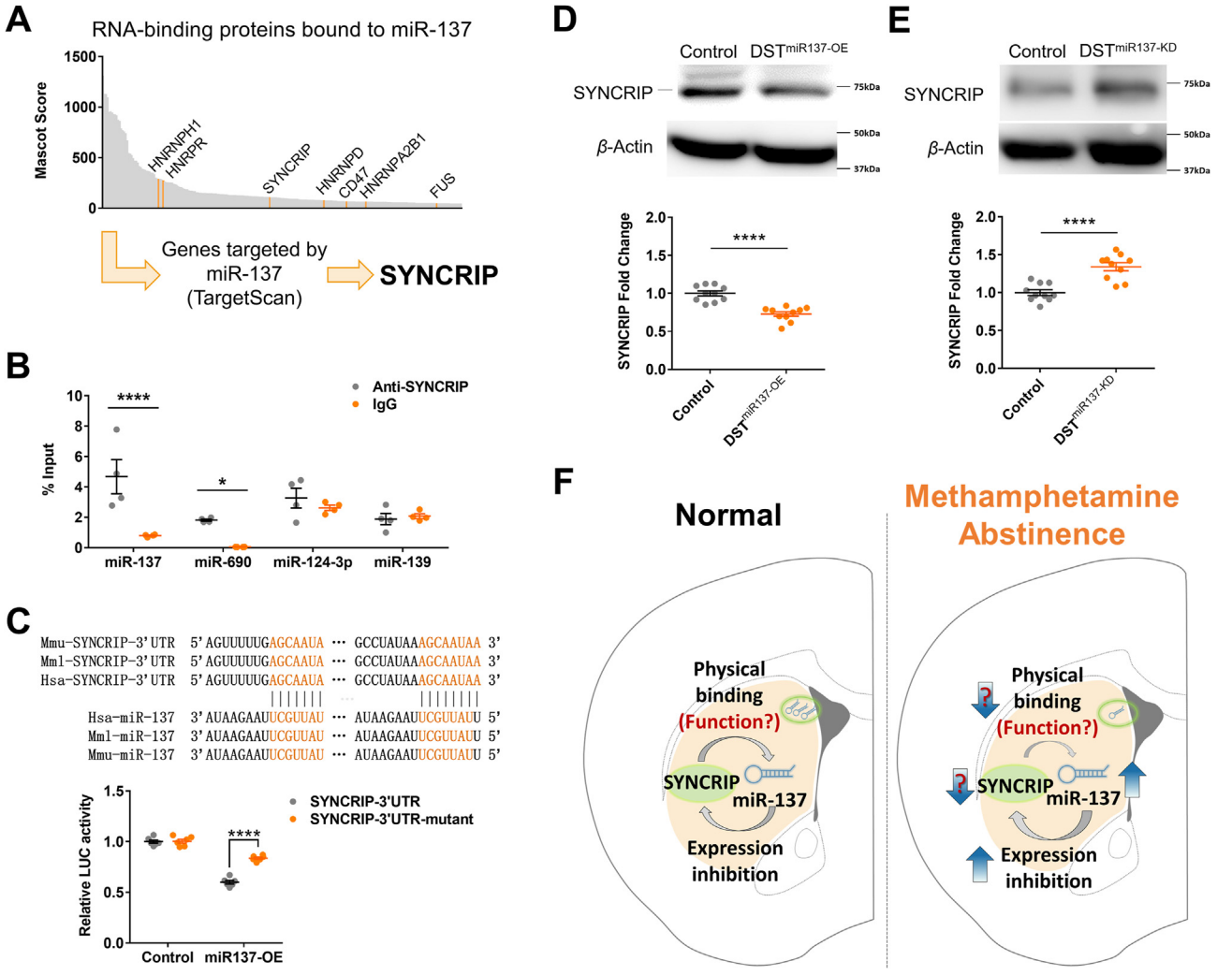

Figure 3 The RNA-binding protein SYNCRIP bidirectionally interacts with miR-137. (A) Through LC−MS/MS proteomics, miR-137-bound RNA-binding proteins (orange) were identified among all proteins pulled down with miR-137. Through bioinformatics, SYNCRIP was identified as a miR-137-bound RNA-binding protein tentatively targeted by miR-137. (B) Through RNA immunoprecipitation (RIP) with SYNCRIP antibody (IgG as control), SYNCRIP-bound miRNAs were isolated and quantified by qPCR as a percentage of the input sample. miR-690 was used as a positive control (a miRNA known to be bound to SYNCRIP), while miR-124-3p and miR-139 were used as negative controls. miR-137 and miR-690 were bound to SYNCRIP, while other miRNAs were not. (C) Above panel shows seed sequence matching between SYNCRIP-3′UTR and miR-137 in *Homo sapiens* (Hsa), *Macaca mulatta* (Mml), and *Mus musculus* (Mmu). Below panel shows luciferase (LUC) assay revealing that SYNCRIP-3′UTR is a direct target of miR-137 (n = 6/group) (Student's t-test). LUC activity from SYNCRIP-3′UTR was significantly reduced by miR-137 overexpression (miR137-OE), and mutation in the SYNCRIP-3′UTR seed sequence (SYNCRIP-3′UTR-mutant) prevented the miR-137-induced reduction in LUC activity. (D) Striatal SYNCRIP protein was significantly reduced after miR-137 overexpression in the dorsal striatum ($DST^{miR137\text{-}OE}$) (n = 10/group) (Student's t-test). (E) Striatal SYNCRIP protein was significantly increased after miR-137 knock-down in the dorsal striatum ($DST^{miR137\text{-}KD}$) (n = 10/group) (Student's t-test). (F) Schematic modeling showing the bidirectional interaction between SYNCRIP and miR-137 in the dorsal striatum. Whether methamphetamine abstinence reduces striatal SYNCRIP and its function remains yet unknown. All error bars represent standard error of the mean. Luciferase assay was performed once, and other experiments were repeated at least once.

proteins (Fig. 3A, orange; Table 1). Then, we compared the seven proteins with the putative targets of miR-137 predicted by TargetScan v7.2[16] and DIANA microT-CDS v5.0[17]. As result, SYNCRIP (Synaptotagmin-binding cytoplasmic RNA interacting protein; also known as HNRNP-Q or NSAP1) was identified as both a miR-137-bound protein as well as a putative target of miR-137 (Fig. 3A, below).

Then, we analyzed brain SYNCRIP-bound miRNAs by RNA immunoprecipitation and qPCR. We quantified miR-137 along with miR-690 (a previously identified miRNA bound to SYNCRIP) as a positive control, and miR-124-3p and miR-139 as negative controls. We found that SYNCRIP physically interacted with miR-137 and miR-690, but not with miR-124-3p or miR-139 (Fig. 3B).

Subsequently, we confirmed whether the 3′UTR of *SYNCRIP* mRNA could be targeted by the seed sequence of miR-137 (Fig. 3C, above), and follow-up experimental validation with luciferase assay confirmed that the expression of *SYNCRIP* mRNA could be repressed by miR-137 (Fig. 3C, below), which replicated the finding from a previous study[31]. Moreover, we confirmed whether miR-137 manipulation in the dorsal striatum could influence the expression pattern of SYNCRIP protein. Immunoblot assay confirmed that $DST^{miR137\text{-}OE}$ diminished striatal SYNCRIP protein (Fig. 3D), whereas $DST^{miR137\text{-}KD}$ enhanced striatal SYNCRIP protein (Fig. 3E).

Lastly, we checked whether MA abstinence altered SYNCRIP in brain regions other than the dorsal striatum, and found that SYNCRIP was unchanged in the neocortex, hippocampus, thalamus, and cerebellum of the mouse model of MA abstinence (Supporting Information Fig. S4E).

These data implied that MA abstinence causes an abnormal increase of striatal miR-137 and inhibits the expression of SYNCRIP, while SYNCRIP is physically bound to miR-137 (Fig. 3F). Here, we speculated from previous studies that striatal SYNCRIP could be mediating MA abstinence-dependent reduction of cEV miR-137 *via* two modes of action: (1) SYNCRIP could sort miR-137 into the exosomes (a type of EVs)[32,33], and (2) SYNCRIP could promote the processing of miR-137[34]. In both scenarios, diminished striatal SYNCRIP function can directly or indirectly reduce striatal EV miR-137 and subsequently cEV miR-137.

Table 1 Proteomic identification of miR-137-bound RNA-binding proteins.

Peptide	Gene nomenclature	Mascot score
Cd47 protein, partial	*CD47*	62
Fusion, derived from t(12;16) malignant liposarcoma (human), isoform CRA_b	*FUS*	58
Heterogenous nuclear ribonucleoprotein A2/B1	*HNRNPA2B1*	43
Hnrnpd protein, partial	*HNRNPD*	46 70 55
Heterogeneous nuclear ribonucleoprotein H1, isoform CRA_b, partial	*HNRNPH1*	281
Hnrpr protein, partial	*HNRPR*	121 268 89 65 140
RRM RNA binding protein NSAP1, partial	*SYNCRIP*	102

3.4. *SYNCRIP mediates the opposite regulation of striatal and circulating miR-137*

We postulated that (1) MA abstinence increased striatal miR-137, (2) inhibited the expression of striatal SYNCRIP, and (3) interrupted the transport of miR-137 into the EVs, which in turn (4) reduced the level of EV-shuttled miR-137 released into the circulation. To examine this model, we first confirmed that MA abstinence led to a reduction of SYNCRIP in the dorsal striatum (Fig. 4A). Second, we confirmed that MA abstinence reduces SYNCRIP in the cEVs (Fig. 4B), which supported the notion that SYNCRIP binds to miRNAs and transports them into the exosomes[32,33].

Third, we adopted PROSPR method to isolate EVs from the dorsal striatum[12], in order to identify how MA abstinence affects miR-137 in the striatal EVs. We found that striatal EVs contained significantly diminished amount of miR-137 after MA abstinence (Fig. 4C). Considering that SYNCRIP sorts miRNAs into the exosomes, our finding suggested that miR-137 sorting into the exosomes may have been negatively regulated by MA abstinence-induced reduction of SYNCRIP.

Thereafter, we investigated whether the change in striatal SYNCRIP is a critical substrate of the MA abstinence-induced reduction of cEV miR-137. We ectopically overexpressed striatal SYNCRIP in the mouse model of MA abstinence ($DST^{SYNCRIP\text{-}OE}$-Abs; Fig. 4D) in order to rescue the diminished expression of SYNCRIP, while other groups of mice received control lentivirus infusion. Interestingly, $DST^{SYNCRIP\text{-}OE}$-Abs exhibited a further increase in the expression of miR-137 in the dorsal striatum (Fig. 4E), which supports the notion that SYNCRIP promotes miR-137 processing to increase the level of mature miR-137[34]. On the other hand, $DST^{SYNCRIP\text{-}OE}$-Abs was able to partially rescue the MA abstinence-induced reduction of cEV miR-137 (Fig. 4F), while the inverse correlation of miR-137 level in the brain and blood was still maintained (Fig. 4G). Furthermore, SYNCRIP overexpression in treatment-naïve cell cultures exhibited simultaneous increases in both cellular and EV miR-137 (Supporting Information Fig. S5). This finding further supported the notion that SYNCRIP facilitates the processing of miR-137.

In sum, these data provided evidence that striatal SYNCRIP is a core component for MA abstinence-dependent reduction of cEV miR-137 most likely *via* miRNA sorting into the exosomes (Fig. 4H). Moreover, our results additionally indicated that cEV miR-137 is persistently reduced during the duration of MA abstinence in both nonhuman primates and mice, and could reflect MA abstinence-induced molecular alterations in the dorsal striatum. Thus, we propose cEV miR-137 as a candidate for the diagnostic marker of MA withdrawal syndrome.

3.5. *Striatal SYNCRIP weakly influences motor behavior*

Despite decades of research on substance-induced disorders, only few of the current pharmacotherapy can effectively counteract the symptoms specific to stimulant abstinence. In addition, behavioral studies on stimulant withdrawal syndrome have primarily focused on the affective-motivational aspect[35].

Stimulant withdrawal syndrome is generally characterized by affective, cognitive, and motor symptoms[1]. The dorsal striatum is involved with cognitive and motor behaviors in animals[36,37]. More

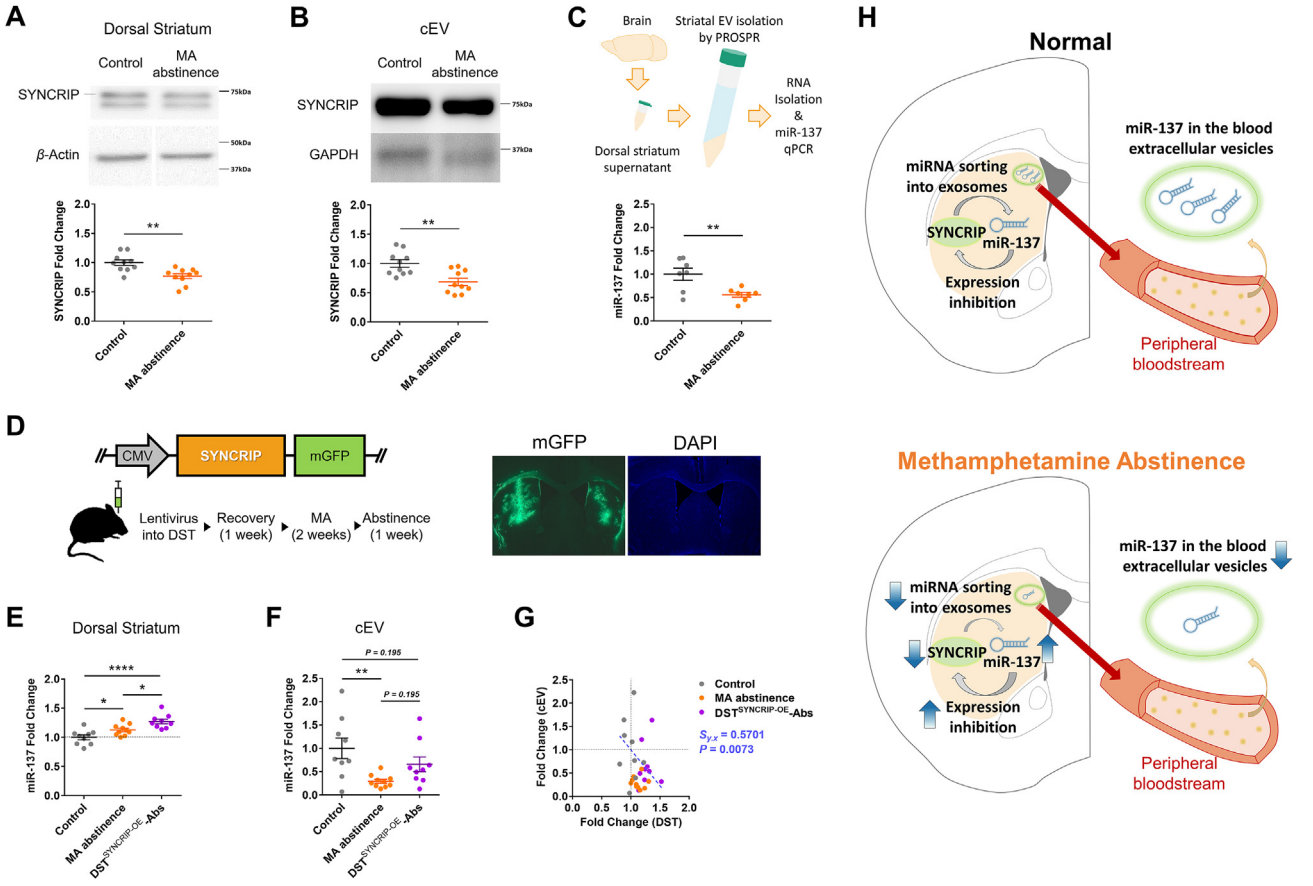

Figure 4 SYNCRIP mediates the MA abstinence-induced reduction of circulating miR-137. (A) Striatal SYNCRIP protein was significantly reduced in the dorsal striatum (DST) of mice after methamphetamine (MA) abstinence (n = 10/group) (Student's t-test). (B) Circulating extracellular vesicle (cEV) SYNCRIP protein was significantly reduced in the DST of mice after MA abstinence (n = 10/group) (Student's t-test). (C) EVs were isolated from the DST by PROSPR method as previously described. miR-137 in the striatal EVs was significantly reduced after MA abstinence (n = 7/group) (Student's t-test). (D) Schedule for lentivirus-mediated overexpression of SYNCRIP in the mouse dorsal striatum ($DST^{SYNCRIP\text{-}OE}$). Images show immunohistochemical confirmation of lentiviral expression in the mouse DST. White bar in the image indicates 1 mm. (E) Quantitative expression level of DST miR-137 was enhanced by MA abstinence. $DST^{SYNCRIP\text{-}OE}$ led to a further increase of miR-137 in the DST of MA-abstinent mice ($DST^{SYNCRIP\text{-}OE}$-Abs) (n = 9−10/group) (Holm-Sidak's *post-hoc* test). (F) cEV miR-137 was rescued by $DST^{SYNCRIP\text{-}OE}$ in the MA-abstinent mice (n = 9−10/group) (Holm-Sidak's *post-hoc* test). (G) miR-137 in the DST was negatively correlated with cEV miR-137 (linear regression). (H) Schematic illustration of the bidirectional interaction between miR-137 and SYNCRIP in the dorsal striatum and its impact on cEV miR-137 during MA abstinence. The increase in striatal miR-137 leads to expression inhibition of SYNCRIP, which reduces the sorting of miR-137 into the exosomes. MA abstinence impedes SYNCRIP-dependent miR-137 sorting into the exosomes, which is reflected in the circulation as a reduction in cEV miR-137. All error bars represent standard error of the mean. All experiments were repeated at least once.

specifically, the dorsal striatum is known to control egocentric spatial learning and motor skill learning[38,39], which are also impaired by MA abstinence in animals[40,41]. Therefore, we explored MA abstinence-induced behavioral dysfunctions specifically focusing on egocentric and motor learning.

Through this study, we aimed to identify the therapeutic potential of SYNCRIP against MA withdrawal syndrome, as proteins are more amenable than RNA for conventional drug discovery approach[42]. Here we compared behavior in four different groups of mice (Supporting Information Fig. S6). In control group, mice were given intrastriatal control lentivirus injection; in $DST^{SYNCRIP\text{-}OE}$ group, striatal SYNCRIP was ectopically overexpressed; in vehicle (Veh) group, mice were given intraperitoneal saline injection; in MA abstinence (Abs) group, the mouse model of MA abstinence was used.

We probed MA abstinence-induced changes in locomotion, motor coordination, spatial navigation strategy, and MA sensitization (Fig. 5A). First, the open field test showed that one week of MA abstinence or SYNCRIP overexpression neither affected baseline locomotion nor anxiety-like behavior (Fig. 5B). Interestingly, hyperactivity and circling count were significantly attenuated by striatal SYNCRIP overexpression in the mouse model of MA abstinence as compared to the control mice, but not compared to the MA-abstinent mice (Supporting Information Fig. S7A and S7B). In addition, the rearing count was not significantly different among all groups (Fig. S7C).

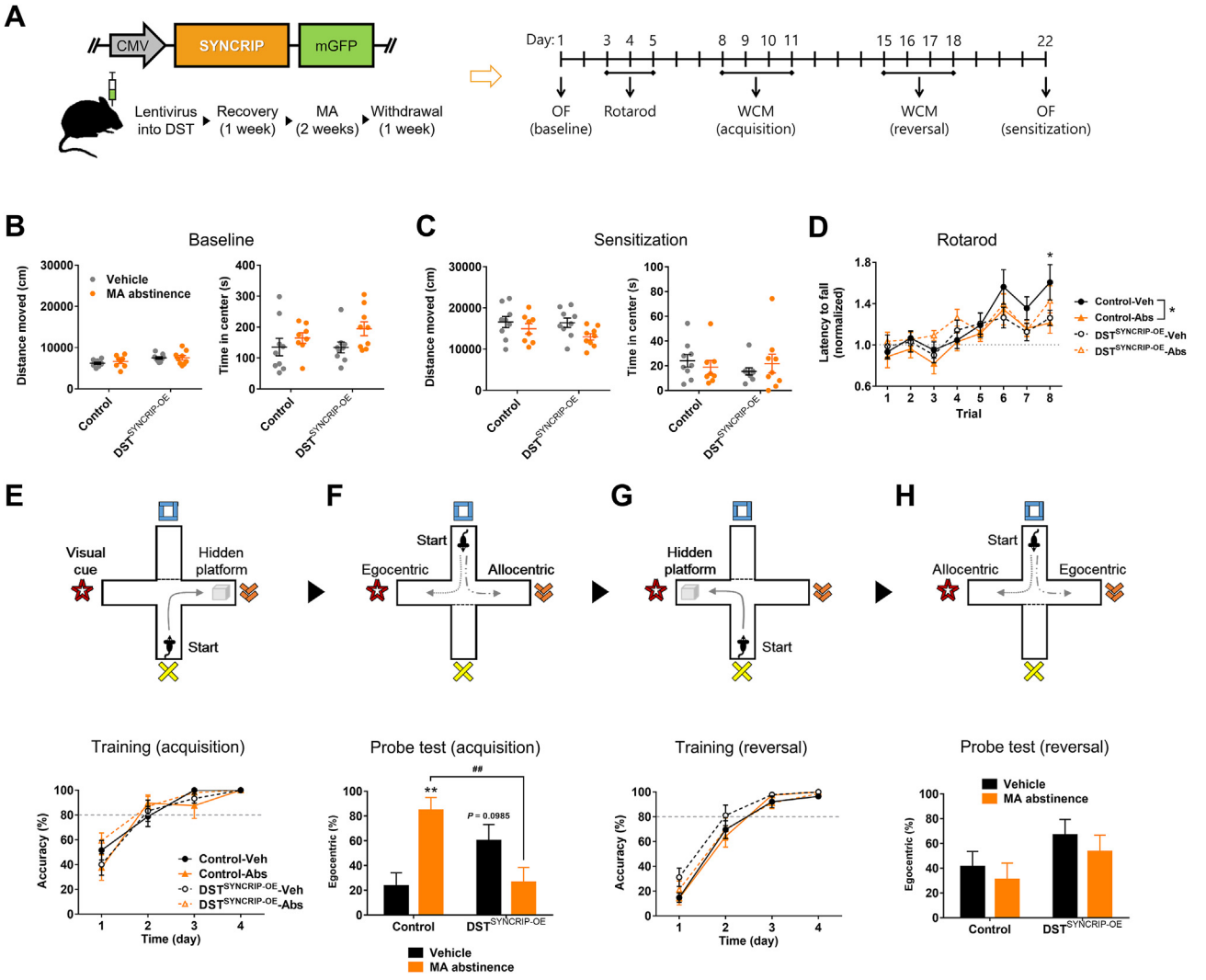

Figure 5 Striatal SYNCRIP controls the MA abstinence-induced increase in egocentric spatial learning. (A) Schedule for behavior tests after lentivirus-mediated overexpression of SYNCRIP in the mouse dorsal striatum (DST). (B) Neither methamphetamine (MA) abstinence nor striatal SYNCRIP overexpression ($DST^{SYNCRIP\text{-}OE}$) affected general locomotor activity or anxiety-like behavior (n = 8–9/group). (C) MA challenge did not affect general locomotor activity and anxiety-like behavior in mice after MA abstinence and/or $DST^{SYNCRIP\text{-}OE}$ (n = 8–9/group). (D) Motor skill learning was slightly impaired by MA abstinence in rotarod test, but $DST^{SYNCRIP\text{-}OE}$ did not have significant effect (n = 9–12/group). (E–H) Water cross maze (WCM) for examination of allocentric/egocentric spatial navigation (n = 13–17/group). Above illustrations show schematic idea of the training/probe trial during the acquisition/reversal phase. (E) Mice did not differ in the training efficiency during the acquisition phase. (F) In acquisition probe test, MA abstinence significantly biased mice towards utilizing egocentric response strategy during spatial navigation, and this effect was fully reversed by $DST^{SYNCRIP\text{-}OE}$ (Holm-Sidak's *post-hoc* test). (G) Mice did not differ in the training efficiency during the reversal phase. (H) Mice did not differ in the proportion of allocentric/egocentric strategy during reversal probe test. All error bars represent standard error of the mean. All experiments were repeated at least once.

Next, the rotarod test showed that MA abstinence weakly impaired motor coordination performance (Fig. 5D), as motor coordination was reduced only at the 8th trial of the rotarod test. In addition, neither MA abstinence nor $DST^{SYNCRIP\text{-}OE}$ significantly affected motor learning (Fig. S7D). These results collectively suggest that MA abstinence did not significantly alter the general locomotor activity or motor skill in mice.

3.6. *Striatal SYNCRIP is necessary for the MA abstinence-induced egocentric spatial navigation bias*

Egocentric spatial navigation specifically requires dorsal striatum-dependent response learning strategy in animals[37,43] and is impaired in response to neurotoxic MA exposure[40]. Therefore, we investigated the impact of MA abstinence and striatal SYNCRIP overexpression on egocentric spatial navigation in the water cross maze (WCM) test.

Neither MA abstinence nor SYNCRIP overexpression affected the acquisition of the location of hidden platform (Fig. 5E). However, mice exhibited vast difference in spatial navigation strategy during the acquisition probe test, as the mouse model of MA abstinence was significantly biased towards adopting egocentric response strategy whereas the control group was more inclined to adopt allocentric place strategy (Fig. 5F, Control–Vehicle *vs.* Control–MA abstinence). Interestingly, ectopic overexpression of striatal SYNCRIP completely prevented the MA abstinence-

induced overrepresentation of the egocentric response learning (Fig. 5F, Control−MA abstinence *vs*. SYNCRIP−MA-abstinence). We next examined whether the reversal learning during WCM test was dysregulated by MA abstinence. In both reversal training and reversal probe test, neither MA abstinence nor SYNCRIP overexpression affected the behavioral outcome (Fig. 5G and H).

Thereafter, we conducted additional analyses to evaluate the effect of MA abstinence or striatal SYNCRIP overexpression on the behavioral parameters relevant to decision making during spatial navigation in the WCM test. The latency to choose an arm did not differ among mice during the probe tests (Supporting Information Fig. S8A). Next, we examined the proportions of decisions to "Stay" *versus* make a "Change-of-mind" during the probe tests (Fig. S8B). The mouse model of MA abstinence was inclined to make the "Stay" decision rather than the "Change-of-mind" decision (Fig. S8C).

Interestingly, in-depth analysis of the navigation strategy adopted during the "Stay" and "Change-of-mind" decisions revealed that mice were more prone to adopt the allocentric space strategy when making the "Change-of-mind" decisions, whereas the spatial navigation strategy was uncertain when making the "Stay" decisions (Fig. S8D). Combining with our result that MA abstinence reduced "Change-of-mind" decisions, these data provide evidence that MA abstinence biased animals to use the egocentric response strategy *via* cognitive inflexibility.

Collectively, these data suggest that MA abstinence caused an abnormal bias towards egocentric response strategy during spatial navigation, which could be fully restored to normal level by rescuing striatal SYNCRIP expression. Taken together, we propose SYNCRIP as a promising therapeutic target for the cognitive aspect of MA withdrawal syndrome.

4. Discussion

4.1. *miR-137 in methamphetamine abstinence*

miR-137 is a brain-enriched and evolutionarily conserved miRNA[20]. miR-137 is a known psychiatric risk gene[44,45] and its genetic variant has cross-disorder effects among multiple psychiatric disorders[46]. For instance, miR-137 was heavily implicated in the pathophysiology of schizophrenia through genome-wide association studies[47,48], but others have also implicated miR-137 in Alzheimer's disease, autism spectrum disorder, and intellectual disability[44,46,49–52].

However, only recently have the studies implicated miR-137 in the pathophysiology of drug abuse[53,54], thus the role of striatal miR-137 in drug abstinence remains largely unknown. Our data indicated that miR-137 is a long-lasting signature of MA abstinence in both brain and blood, suggesting that miR-137 could play a multifaceted role within the system undergoing MA abstinence. As previous studies revealed that miR-137 plays a role in molecular processes such as neurodevelopment[55,56] and synaptic plasticity[45,57], it would be interesting to study striatal miR-137 in the context of the relationship between neural functions and withdrawal syndrome or incubation of drug craving[58,59].

4.2. *SYNCRIP in methamphetamine abstinence*

SYNCRIP is an RNA-binding protein that functions to sort miRNAs into exosomes[32,33]. A seminal study revealed that SYNCRIP interacts with synaptotagmin, the core component of synaptic vesicle exocytosis[60,61]. Following this finding, studies have sequentially demonstrated that SYNCRIP is involved in synapse formation and synaptic plasticity[62,63].

Only recently have the studies begun to uncover the behavioral functions of SYNCRIP. An animal model study showed that SYNCRIP controls starvation-induced hyperactivity in drosophila[64], while a case report proposed that *de novo* variants in SYNCRIP is linked to neurodevelopmental disorders[65]. However, the association between SYNCRIP and behavioral functions as well as dysfunctions remains largely unclear to date.

In this study, we found that SYNCRIP is related to the cognitive symptoms of MA abstinence, namely the behavioral bias towards egocentric learning during spatial navigation. Moreover, our data indicate that SYNCRIP could be linked to motor learning deficit induced by MA abstinence. These data indicate that it would be interesting to study how SYNCRIP-dependent control of striatal synaptic plasticity and morphology affects behavior during MA abstinence.

4.3. *SYNCRIP-dependent regulation of miRNA miR-137*

SYNCRIP is an RNA-binding protein that can control miRNA in various ways. Here we found that SYNCRIP enhances both cellular and EV miR-137. Various modes of action can influence this phenomenon: (1) SYNCRIP-dependent sorting of miRNAs into the exosomes, (2) SYNCRIP-dependent enhancement in the processing of miRNAs, and (3) SYNCRIP-mediated localization of miRNAs into a specific compartment within a cell.

First, SYNCRIP is known to sort miRNAs into the exosomes[32], a type of EVs, and previous studies as well as our data have demonstrated that EVs can protect the cargo RNAs from degradation[29,66]. These findings suggest that SYNCRIP overexpression could enhance the sorting of miR-137 into the exosomes. Then, the intracellular EVs (not yet released) would protect striatal miR-137 from degradation and hence lead to an "increased" level of striatal miR-137 due to the reduced degradation. Interestingly, previous studies demonstrated that SYNCRIP binds to a specific set of miRNAs mainly by recognizing GGCU sequence[32,33], but indicated that SYNCRIP could also recognize GGYU sequence. Mature miR-137 contains GGGU sequence, a putative SYNCRIP binding motif. This supports the possibility that SYNCRIP sorts miR-137 into the exosomes. Interestingly, our data show that MA abstinence reduced striatal SYNCRIP and simultaneously reduced striatal EV miR-137, suggesting that SYNCRIP may be required for sorting miR-137 into the exosomes.

Second, SYNCRIP is known to either promote or silence the processing of a set of miRNAs *via* either association with DGCR8 or direct interaction with primary miRNAs[34]. Then, SYNCRIP overexpression might simply promote the processing of striatal miR-137, leading to increased expression of striatal miR-137. The increased expression of striatal miR-137 would then enter into the EVs, since the EV cargo comes from the cytoplasmic content of the originating cell/tissue. Our data also supported that SYNCRIP facilitates the processing of miR-137, as SYNCRIP overexpression enhanced miR-137 *in vivo* and *in vitro*. However, we cannot exclude the possibility that SYNCRIP sorting of miR-137 into the EVs induced the increase in striatal miR-137, as the EVs would protect striatal miR-137 from degradation and hence "increase" (reduce the degradation of) striatal miR-137.

Third, SYNCRIP transports RNAs into a specific location within a cell. Previous studies demonstrated that SYNCRIP functions as a module that binds to and transports mRNAs to the

dendritic compartment as a component of mRNA granule[67,68], which may result in changes relevant to the MA abstinence-dependent reduction of cEV miR-137d. However, whether the mRNA transport function of SYNCRIP extends to miR-137 has not been explored to date, including in this study. Also, miR-137 was shown to be preferentially localized within the cytoplasmic compartment rather than dendrites[69]. This finding suggests that SYNCRIP is not likely to transport miR-137 to the dendritic compartment.

4.4. *Bidirectional interaction between miR-137 and SYNCRIP*

Here, we found that miR-137 inhibits the expression of SYNCRIP protein while SYNCRIP physically binds to miR-137. Such bidirectional interaction suggests that SYNCRIP and miR-137 could be functionally associated with each other. For instance, this study demonstrated that both miR-137 and SYNCRIP in the dorsal striatum could control the expression of cEV miR-137, while our previous study demonstrated that the inhibitory homeostatic relationship between striatal MeCP2 and miR-212 controls cocaine intake[70]. Extending this idea, as SYNCRIP is involved in miRNA sorting into the EVs and interacts with the synapse- and long-term potentiation-associated protein synaptotagmin[45,61], miR-137 might also play a part in EV miRNA sorting and long-term potentiation. *Vice versa*, SYNCRIP might also be involved in the function and dysfunction mediated by miR-137, such as neural development and schizophrenia.

4.5. *Implications from SYNCRIP as a regulator of circulating miRNAs*

We found that the brain was actively engaged in the control of the miRNA content in the circulation *via* the RNA-binding protein SYNCRIP. This suggests that the RNA-binding protein-dependent brain-to-blood transfer of RNAs may be a universal phenomenon among animals. This idea opens up an interesting possibility that RNA-binding proteins such as SYNCRIP may be essential for the translational discovery of mechanism-based markers that can reveal the state of the diseased brain.

Recent studies brought advances in the method to comprehensively assess the interactions between RNA-binding proteins and their target RNAs, for instance, the RNA interactome capture method[71]. Combined with the efforts to identify disease-relevant RNA-binding proteins in a specific organ, it would be possible to accelerate the identification of a large pool of circulating RNAs that can reflect the state of diseased organs.

4.6. *Limitations and further study*

We focused on the molecular interaction between miR-137 and SYNCRIP, and translated our data for theragnosis of MA abstinence. As discussed in a previous review[42], protein targets (*e.g.*, SYNCRIP) are generally more amenable to conventional drug discovery while RNA targets (*e.g.*, miR-137) are not. This limitation led us to focus on the therapeutic role of SYNCRIP on behavior rather than miR-137. This does not exclude the possibility that miR-137 could play crucial roles in the aberrant behaviors and neuropathological mechanisms relevant to MA abstinence as well as addiction. In a continuing line of study, the role of miR-137 on MA abstinence should be examined in the future.

Intriguingly, we found that MA abstinence-dependent increase in striatal miR-137 was further enhanced by striatal SYNCRIP overexpression, but it did not prevent SYNCRIP from rescuing MA abstinence-induced behavioral bias towards egocentric learning. These findings propose that (1) striatal miR-137 might not underlie egocentric learning, or that (2) SYNCRIP did not actually enhance the level of miR-137. In the second scenario, SYNCRIP sorts miR-137 into the EVs, which might lead to enhanced protection of miR-137 from degradation mechanisms and hence "increase" striatal miR-137. In any case, further studies are required to identify the role of striatal miR-137 on behavior.

Here we also focused on the identification of theranostic targets for MA abstinence, which required systems-level (brain and blood) observations. As such, the cell-type-specific roles that miR-137 and SYNCRIP play during MA abstinence were largely neglected in this study. Further studies should reveal the cell-type-specific expression patterns of miR-137 and SYNCRIP in the brain (*e.g.*, in neurons, astrocytes, and microglia), the differential roles that they play in neurons and glia, and their cell-type-specific effect on behavior.

In this study, the function of cEV miR-137 during MA abstinence has not been explored in-depth, which could be crucial for understanding how the brain-derived molecules affect the periphery. A number of factors should be considered when manipulating the miRNAs in the circulating EVs. First, EVs express different sets of membrane proteins and cargo depending on their originating cell type, thereby echoing the phenotype of their parent cell[72]. Second, the membrane proteins of EVs are especially important since they decide the tissue type that the EVs are targeting[73]. Therefore, simply injecting miRNA- or antagomiR-filled EVs into the circulation would not be able to mimic or inhibit the function of endogenous cEV miRNAs. Tissue-specific targeting profile of brain-derived EVs in the circulation is a prerequisite, and would be an important topic to visit in the field of EV biology.

Lastly, how drug abstinence or addiction alters the physical and biological properties of EVs such as exosomes would be an intriguing topic to explore. A previous study found that MA exposure facilitates the release of endothelial-derived microparticles into the plasma[74]. This suggests that MA abstinence might also affect the size distribution and number of EVs in the brain or blood, which may impact both cell-to-cell communication in the brain and the search for circulating markers of human diseases.

5. Conclusions

Here we laid out how miRNA−target interaction in the dorsal striatum controls brain-to-blood miRNA release and striatum-dependent behaviors during MA abstinence. Our data provided evidence that MA abstinence aberrantly regulates the striatal miRNA−target interaction, specifically the bidirectional interaction between miR-137 and SYNCRIP. miR-137 inhibited the expression of SYNCRIP, while SYNCRIP likely controlled miR-137 in two modes: (1) enhancing intracellular miR-137 expression, and (2) orchestrating exosome release. Lastly, SYNCRIP was identified to mediate MA abstinence-dependent bias in spatial navigation towards egocentric strategy. These data shed light on the roles that SYNCRIP plays in EV miRNA biology, which opens the way for studying cell-to-cell communication and its dysfunction in brain diseases. Consequently, our data paved the way for the development of mechanism-based theranostics against MA withdrawal syndrome. From our findings, we proposed (1) cEV miR-137 as a potential mechanism-based marker of MA

abstinence that can reveal the changes in striatal miR-137/SYNCRIP interaction, and (2) striatal SYNCRIP as a potential therapeutic target for the cognitive aspect of MA withdrawal syndrome. Moreover, our study showed that exploiting the brain-specific miRNA−target interaction could accelerate the search for the theranostic targets of brain diseases. These notions warrant future studies to develop effective theranostics against MA withdrawal syndrome as well as other human brain diseases.

Acknowledgments

This research was funded by Korea Institute of Science and Technology Intramural Funding (2E26640, 2E30952; Republic of Korea), National Research Council of Science & Technology (NST) grant by Korean government (MSIP) (CRC-15-04-KIST; Republic of Korea), Center for Women In Science, Engineering, and Technology (WISET) grant by Korean government (WISET2020-525; Republic of Korea), National Research Foundation of Korea (2017R1A2B2003993, 2020R1A2C2004610; Republic of Korea), and UST Young Scientist Research Program through Korea University of Science and Technology (UST) (2017YS03; Republic of Korea).

Author contributions

Baeksun Kim: project administration, conceptualization, methodology, funding acquisition, investigation, validation, visualization, formal analysis, data curation, writing-original draft, and writing-review & editing. Sung Hyun Tag: methodology, investigation, validation, visualization, formal analysis, and data curation. Eunjoo Nam: funding acquisition and investigation. Suji Ham: investigation. Sujin Ahn: investigation. Juhwan Kim: investigation. Doo-Wan Cho: methodology and data curation. Sangjoon Lee: investigation. Young-Su Yang: investigation. Seung Eun Lee: investigation. Yong Sik Kim: supervision. Il-Joo Cho: supervision. Kwang Pyo Kim: supervision, resources, formal analysis. Su-Cheol Han: supervision, resources. Heh-In Im: supervision, project administration, conceptualization, methodology, funding acquisition, resources, writing-original draft, and writing-review & editing.

Conflicts of interest

The authors declare no conflict of interest.

Appendix A. Supporting information

Supporting data to this article can be found online at https://doi.org/10.1016/j.apsb.2022.02.030.

References

1. American Psychiatric Association. *Diagnostic and statistical manual of mental disorders (DSM-5®)*. 5th ed. American Psychiatric Publishing; 2013.
2. McGregor C, Srisurapanont M, Jittiwutikarn J, Laobhripatr S, Wongtan T, White JM. The nature, time course and severity of methamphetamine withdrawal. *Addiction* 2005;**100**:1320−9.
3. Paulson PE, Robinson TE. Regional differences in the effects of amphetamine withdrawal on dopamine dynamics in the striatum. *Neuropsychopharmacology* 1996;**14**:325−37.
4. Chang L, Alicata D, Ernst T, Volkow N. Structural and metabolic brain changes in the striatum associated with methamphetamine abuse. *Addiction* 2007;**102**:16−32.
5. Gowen AM, Odegaard KE, Hernandez J, Chand S, Koul S, Pendyala G, et al. Role of microRNAs in the pathophysiology of addiction. *Wiley Interdiscip Rev RNA* 2021;**12**:e1637.
6. Bartel DP. MicroRNAs: genomics, biogenesis, mechanism, and function. *Cell* 2004;**116**:281−97.
7. O'neil ML, Kuczenski R, Segal DS, Cho AK, Lacan G, Melega WP. Escalating dose pretreatment induces pharmacodynamic and not pharmacokinetic tolerance to a subsequent high-dose methamphetamine binge. *Synapse* 2006;**60**:465−73.
8. Segal DS, Kuczenski R, O'Neil ML, Melega WP, Cho AK. Escalating dose methamphetamine pretreatment alters the behavioral and neurochemical profiles associated with exposure to a high-dose methamphetamine binge. *Neuropsychopharmacology* 2003;**28**:1730.
9. Madden LJ, Flynn CT, Zandonatti MA, May M, Parsons LH, Katner SN, et al. Modeling human methamphetamine exposure in nonhuman primates: chronic dosing in the rhesus macaque leads to behavioral and physiological abnormalities. *Neuropsychopharmacology* 2005;**30**:350−9.
10. Groman SM, Lee B, Seu E, James AS, Feiler K, Mandelkern MA, et al. Dysregulation of D2-mediated dopamine transmission in monkeys after chronic escalating methamphetamine exposure. *J Neurosci* 2012;**32**:5843−52.
11. Kesby JP, Heaton RK, Young JW, Umlauf A, Woods SP, Letendre SL, et al. Methamphetamine exposure combined with HIV-1 disease or gp120 expression: comparison of learning and executive functions in humans and mice. *Neuropsychopharmacology* 2015;**40**:1899.
12. Gallart-Palau X, Serra A, Sze SK. Enrichment of extracellular vesicles from tissues of the central nervous system by PROSPR. *Mol Neurodegener* 2016;**11**:41.
13. Livak KJ, Schmittgen TD. Analysis of relative gene expression data using real-time quantitative PCR and the $2^{-\Delta\Delta CT}$ method. *Methods* 2001;**25**:402−8.
14. Gobom J, Nordhoff E, Mirgorodskaya E, Ekman R, Roepstorff P. Sample purification and preparation technique based on nano-scale reversed-phase columns for the sensitive analysis of complex peptide mixtures by matrix-assisted laser desorption/ionization mass spectrometry. *J Mass Spectrom* 1999;**34**:105−16.
15. Perkins DN, Pappin DJ, Creasy DM, Cottrell JS. Probability-based protein identification by searching sequence databases using mass spectrometry data. *Electrophoresis* 1999;**20**:3551−67.
16. Agarwal V, Bell GW, Nam JW, Bartel DP. Predicting effective microRNA target sites in mammalian mRNAs. *eLife* 2015;**4**:e05005.
17. Paraskevopoulou MD, Georgakilas G, Kostoulas N, Vlachos IS, Vergoulis T, Reczko M, et al. DIANA-microT web server v5.0: service integration into miRNA functional analysis workflows. *Nucleic Acids Res* 2013;**41**:W169−73.
18. Kim B, Im HI. Chronic nicotine impairs sparse motor learning *via* striatal fast-spiking parvalbumin interneurons. *Addiction Biol* 2021;**26**:e12956.
19. Pepe MS, Longton G, Anderson GL, Schummer M. Selecting differentially expressed genes from microarray experiments. *Biometrics* 2003;**59**:133−42.
20. Sempere LF, Freemantle S, Pitha-Rowe I, Moss E, Dmitrovsky E, Ambros V. Expression profiling of mammalian microRNAs uncovers a subset of brain-expressed microRNAs with possible roles in murine and human neuronal differentiation. *Genome Biol* 2004;**5**:R13.
21. Yáñez-Mó M, Siljander PR-M, Andreu Z, Bedina Zavec A, Borràs FE, Buzas EI, et al. Biological properties of extracellular vesicles and their physiological functions. *J Extracell Vesicles* 2015;**4**:27066.
22. Alvarez-Erviti L, Seow Y, Yin H, Betts C, Lakhal S, Wood MJ. Delivery of siRNA to the mouse brain by systemic injection of targeted exosomes. *Nat Biotechnol* 2011;**29**:341−5.
23. Ridder K, Keller S, Dams M, Rupp A-K, Schlaudraff J, Del Turco D, et al. Extracellular vesicle-mediated transfer of genetic information between the hematopoietic system and the brain in response to inflammation. *PLoS Biol* 2014;**12**:e1001874.

24. Théry C, Witwer KW, Aikawa E, Alcaraz MJ, Anderson JD, Andriantsitohaina R, et al. Minimal information for studies of extracellular vesicles 2018 (MISEV2018): a position statement of the International Society for Extracellular Vesicles and update of the MISEV2014 guidelines. *J Extracell Vesicles* 2018;**7**:1535750.
25. Gualerzi A, Kooijmans SAA, Niada S, Picciolini S, Brini AT, Camussi G, et al. Raman spectroscopy as a quick tool to assess purity of extracellular vesicle preparations and predict their functionality. *J Extracell Vesicles* 2019;**8**:1568780.
26. Kowal J, Arras G, Colombo M, Jouve M, Morath JP, Primdal-Bengtson B, et al. Proteomic comparison defines novel markers to characterize heterogeneous populations of extracellular vesicle subtypes. *Proc Natl Acad Sci U S A* 2016;**113**:E968−77.
27. Ge Q, Zhou Y, Lu J, Bai Y, Xie X, Lu Z. miRNA in plasma exosome is stable under different storage conditions. *Molecules* 2014;**19**:1568−75.
28. Scofield M, Heinsbroek J, Gipson C, Kupchik Y, Spencer S, Smith A, et al. The nucleus accumbens: mechanisms of addiction across drug classes reflect the importance of glutamate homeostasis. *Pharmacol Rev* 2016;**68**:816−71.
29. Zhang J, Li S, Li L, Li M, Guo C, Yao J, et al. Exosome and exosomal microRNA: trafficking, sorting, and function. *Genom Proteom Bioinf* 2015;**13**:17−24.
30. O'Brien K, Breyne K, Ughetto S, Laurent LC, Breakefield XO. RNA delivery by extracellular vesicles in mammalian cells and its applications. *Nat Rev Mol Cell Biol* 2020;**21**:585−606.
31. He E, Lozano MAG, Stringer S, Watanabe K, Sakamoto K, den Oudsten F, et al. MIR137 schizophrenia-associated locus controls synaptic function by regulating synaptogenesis, synapse maturation and synaptic transmission. *Hum Mol Genet* 2018;**27**:1879−91.
32. Santangelo L, Giurato G, Cicchini C, Montaldo C, Mancone C, Tarallo R, et al. The RNA-binding protein SYNCRIP is a component of the hepatocyte exosomal machinery controlling microRNA sorting. *Cell Rep* 2016;**17**:799−808.
33. Hobor F, Dallmann A, Ball NJ, Cicchini C, Battistelli C, Ogrodowicz RW, et al. A cryptic RNA-binding domain mediates Syncrip recognition and exosomal partitioning of miRNA targets. *Nat Commun* 2018;**9**:1−16.
34. Chen Y, Chan J, Chen W, Li J, Sun M, Kannan GS, et al. SYNCRIP, a new player in pri-let-7a processing. *RNA* 2020;**26**:290−305.
35. Koob GF, Le Moal M. Drug addiction, dysregulation of reward, and allostasis. *Neuropsychopharmacology* 2001;**24**:97−129.
36. Dudman JT, Krakauer JW. The basal ganglia: from motor commands to the control of vigor. *Curr Opin Neurobiol* 2016;**37**:158−66.
37. Yin HH, Knowlton BJ. Contributions of striatal subregions to place and response learning. *Learn Mem* 2004;**11**:459−63.
38. Klaus A, Alves da Silva J, Costa RM. What, if, and when to move: basal ganglia circuits and self-paced action initiation. *Annu Rev Neurosci* 2019;**42**:459−83.
39. Chersi F, Burgess N. The cognitive architecture of spatial navigation: hippocampal and striatal contributions. *Neuron* 2015;**88**:64−77.
40. Herring NR, Schaefer TL, Gudelsky GA, Vorhees CV, Williams MT. Effect of (+)-methamphetamine on path integration learning, novel object recognition, and neurotoxicity in rats. *Psychopharmacology* 2008;**199**:637−50.
41. Huang X, Chen Y-Y, Shen Y, Cao X, Li A, Liu Q, et al. Methamphetamine abuse impairs motor cortical plasticity and function. *Mol Psychiatr* 2017;**22**:1274−81.
42. Ha J, Park H, Park J, Park SB. Recent advances in identifying protein targets in drug discovery. *Cell Chem Biol* 2021;**28**:394−423.
43. Packard MG, McGaugh JL. Inactivation of hippocampus or caudate nucleus with lidocaine differentially affects expression of place and response learning. *Neurobiol Learn Mem* 1996;**65**:65−72.
44. Cheng Y, Wang Z-M, Tan W, Wang X, Li Y, Bai B, et al. Partial loss of psychiatric risk gene *Mir 137* in mice causes repetitive behavior and impairs sociability and learning *via* increased Pde10a. *Nat Neurosci* 2018;**21**:1689−703.
45. Siegert S, Seo J, Kwon EJ, Rudenko A, Cho S, Wang W, et al. The schizophrenia risk gene product miR-137 alters presynaptic plasticity. *Nat Neurosci* 2015;**18**:1008.
46. Consortium C-DGotPG. Identification of risk loci with shared effects on five major psychiatric disorders: a genome-wide analysis. *Lancet* 2013;**381**:1371−9.
47. Ripke S, O'Dushlaine C, Chambert K, Moran JL, Kähler AK, Akterin S, et al. Genome-wide association analysis identifies 13 new risk loci for schizophrenia. *Nat Genet* 2013;**45**:1150.
48. Ripke S, Sanders AR, Kendler KS, Levinson DF, Sklar P, Holmans PA, et al. Genome-wide association study identifies five new schizophrenia loci. *Nat Genet* 2011;**43**:969−76.
49. Geekiyanage H, Chan C. MicroRNA-137/181c regulates serine palmitoyltransferase and in turn amyloid β, novel targets in sporadic Alzheimer's disease. *J Neurosci* 2011;**31**:14820−30.
50. Mahmoudi E, Cairns M. MiR-137: an important player in neural development and neoplastic transformation. *Mol Psychiatr* 2017;**22**:44−55.
51. Pinto D, Delaby E, Merico D, Barbosa M, Merikangas A, Klei L, et al. Convergence of genes and cellular pathways dysregulated in autism spectrum disorders. *Am J Hum Genet* 2014;**94**:677−94.
52. Willemsen MH, Vallès A, Kirkels LA, Mastebroek M, Loohuis NO, Kos A, et al. Chromosome 1p21. 3 microdeletions comprising *DPYD* and *MIR137* are associated with intellectual disability. *J Med Genet* 2011;**48**:810−8.
53. Quinn RK, James MH, Hawkins GE, Brown AL, Heathcote A, Smith DW, et al. Temporally specific miRNA expression patterns in the dorsal and ventral striatum of addiction-prone rats. *Addiction Biol* 2018;**23**:631−42.
54. Cabana-Dominguez J, Arenas C, Cormand B, Fernandez-Castillo N. MiR-9, miR-153 and miR-124 are down-regulated by acute exposure to cocaine in a dopaminergic cell model and may contribute to cocaine dependence. *Transl Psychiatr* 2018;**8**:1−8.
55. Sun G, Ye P, Murai K, Lang M-F, Li S, Zhang H, et al. miR-137 forms a regulatory loop with nuclear receptor TLX and LSD1 in neural stem cells. *Nat Commun* 2011;**2**:529.
56. Smrt RD, Szulwach KE, Pfeiffer RL, Li X, Guo W, Pathania M, et al. MicroRNA miR-137 regulates neuronal maturation by targeting ubiquitin ligase mind bomb-1. *Stem Cell* 2010;**28**:1060−70.
57. Loohuis NFO, Ba W, Stoerchel PH, Kos A, Jager A, Schratt G, et al. MicroRNA-137 controls AMPA-receptor-mediated transmission and mGluR-dependent LTD. *Cell Rep* 2015;**11**:1876−84.
58. Newton TF, Kalechstein AD, Duran S, Vansluis N, Ling W. Methamphetamine abstinence syndrome: preliminary findings. *Am J Addict* 2004;**13**:248−55.
59. Pickens CL, Airavaara M, Theberge F, Fanous S, Hope BT, Shaham Y. Neurobiology of the incubation of drug craving. *Trends Neurosci* 2011;**34**:411−20.
60. Martens S, Kozlov MM, McMahon HT. How synaptotagmin promotes membrane fusion. *Science* 2007;**316**:1205−8.
61. Mizutani A, Fukuda M, Ibata K, Shiraishi Y, Mikoshiba K. SYNCRIP, a cytoplasmic counterpart of heterogeneous nuclear ribonucleoprotein R, interacts with ubiquitous synaptotagmin isoforms. *J Biol Chem* 2000;**275**:9823−31.
62. Titlow J, Robertson F, Järvelin A, Ish-Horowicz D, Smith C, Gratton E, et al. Syncrip/hnRNP Q is required for activity-induced Msp300/Nesprin-1 expression and new synapse formation. *J Cell Biol* 2020;**219**:e201903135.
63. Halstead JM, Lin YQ, Durraine L, Hamilton RS, Ball G, Neely GG, et al. Syncrip/hnRNP Q influences synaptic transmission and regulates BMP signaling at the *Drosophila* neuromuscular synapse. *Biol Open* 2014;**3**:839−49.
64. Chi W, Liu W, Fu W, Xia S, Heckscher ES, Zhuang X. RNA-binding protein Syncrip regulates starvation-induced hyperactivity in adult *Drosophila*. *PLoS Genet* 2021;**17**:e1009396.
65. Semino F, Schröter J, Willemsen MH, Bast T, Biskup S, Beck-Woedl S, et al. Further evidence for *de novo* variants in SYNCRIP as

the cause of a neurodevelopmental disorder. *Hum Mutat* 2021;**42**:1094−100.
66. Kim KM, Abdelmohsen K, Mustapic M, Kapogiannis D, Gorospe M. RNA in extracellular vesicles. *Wiley Interdiscip Rev RNA* 2017;**8**:e1413.
67. Bannai H, Fukatsu K, Mizutani A, Natsume T, Iemura SI, Ikegami T, et al. An RNA-interacting protein, SYNCRIP (heterogeneous nuclear ribonuclear protein Q1/NSAP1) is a component of mRNA granule transported with inositol 1,4,5-trisphosphate receptor type 1 mRNA in neuronal dendrites. *J Biol Chem* 2004;**279**:53427−34.
68. McDermott SM, Meignin C, Rappsilber J, Davis I. *Drosophila* Syncrip binds the gurken mRNA localisation signal and regulates localised transcripts during axis specification. *Biol Open* 2012;**1**:488−97.
69. Li Y, Wang J, Chen S, Wu P, Xu S, Wang C, et al. miR-137 boosts the neuroprotective effect of endothelial progenitor cell-derived exosomes in oxyhemoglobin-treated SH-SY5Y cells partially *via* COX2/PGE2 pathway. *Stem Cell Res Ther* 2020;**11**:1−18.
70. Im HI, Hollander JA, Bali P, Kenny PJ. MeCP2 controls BDNF expression and cocaine intake through homeostatic interactions with microRNA-212. *Nat Neurosci* 2010;**13**:1120−7.
71. Perez-Perri JI, Noerenberg M, Kamel W, Lenz CE, Mohammed S, Hentze MW, et al. Global analysis of RNA-binding protein dynamics by comparative and enhanced RNA interactome capture. *Nat Protoc* 2021;**16**:27−60.
72. Katsuda T, Kosaka N, Takeshita F, Ochiya T. The therapeutic potential of mesenchymal stem cell-derived extracellular vesicles. *Proteomics* 2013;**13**:1637−53.
73. Vader P, Mol EA, Pasterkamp G, Schiffelers RM. Extracellular vesicles for drug delivery. *Adv Drug Deliv Rev* 2016;**106**:148−56.
74. Nazari A, Zahmatkesh M, Mortaz E, Hosseinzadeh S. Effect of methamphetamine exposure on the plasma levels of endothelial-derived microparticles. *Drug Alcohol Depend* 2018;**186**:219−25.